

# Microwaves in dispersive magnetic composite media

(Review Article)

S.I. Tarapov

*Institute of Radiophysics and Electronics National Academy of Sciences of Ukraine, 12 Ac. Proskura Str., Kharkov 61085, Ukraine*

E-mail: tarapov@ire.kharkov.ua

D.P. Belozorov

*Institute for Theoretical Physics, National Science Center “Kharkov Institute of Physics and Technology”*

*National Academy of Sciences of Ukraine, 1 Akademicheskaja Str., Kharkov 61108, Ukraine*

Received March 12, 2012

Review discusses some special questions of physics of composite media (metamaterials), which are formed by elements made from natural materials of two kinds. The first ones are “carriers of permittivity” and are presented by plasma-like media and semiconductors. The second ones are “carriers of permeability” — they are presented by ferromagnets. Among such ferromagnets are ferroelectrics (ferrites) and manganite-perovskite compounds. In the first chapter of the review some principal aspects of the electrodynamics of periodical structures — magnetophotonic crystals are considered. The questions of zone structure and possible violations of periodicity (Tamm states, defect mode) as well as the influence of external magnetic field on the spectral characteristics of magnetophotonic crystals are considered. The second chapter of the review is devoted to the electrodynamics of left-handed media (left-handed metamaterials). Different versions of composite left-handed media are considered. Particular attention is paid to features of electrodynamics of artificially synthesized left-handed media, the doped lanthanum manganites-perovskites, which in a certain concentrations of doping element and temperature range can serve as an example of natural left-handed media. The Appendix describes the details of experimental techniques radiophysical research. Note that the research and design of the metamaterials listed above in a range of low temperatures are particularly important. This is due to the fact that at low temperatures a main disadvantage of artificial materials mentioned above (quite large losses) becomes less noticeable. At the same time the main their advantage (namely the possibility to control their frequency dispersion) remains. Thus it seems that the most prospective areas of application and further study of the magnetic metamaterials lie at low temperatures.

PACS: 75.50.–y Magnetic materials;  
78.67.Pt Metamaterials;  
41.20.Jb Microwave radiation wave propagation.

Keywords: magnetic metamaterials, permeability frequency dispersion, permittivity, microwaves.

## Contents

1. INTRODUCTION .....	767
2. PHOTONIC CRYSTALS, EFFECTS OF INHOMOGENEITY .....	768
2.1. Magnetically controllable 1D magnetophotonic crystal .....	768
2.2. Defect mode in magnetophotonic crystal with ferrite defect element .....	771
2.3. Defect mode in magnetophotonic crystal with semiconductor defect element .....	771
2.4. Tamm states in magnetophotonic crystals and permittivity of the wire medium .....	773
2.5. Tamm states on the interface of two photonic crystals .....	774
2.6. Tamm states on the interface of magnetophotonic crystal and semiconductor .....	775
2.7. Peculiarities of the magnetic periodic multilayered ferrite-semiconductor structures .....	776
3. MEDIA WITH NEGATIVE REFRACTION .....	777
3.1. Formation of backward wave in a metamaterial .....	777
3.2. Transmission of electromagnetic waves in a fine-stratified ferrite/semiconductor structure .....	779
3.3. Left-handed properties of semiconductor/ferrite composite. Transparency improving .....	781

3.4. The negative refraction in ferrite/semiconductor composite .....	782
3.5. Left-handed properties of ferrite/metal based composites (ferrite/wire medium, ferrite/thin metal plates) .....	783
3.6. Left-handed behavior of strontium-doped lanthanum manganite .....	784
3.7. Dispersion of negative permittivity of strontium-doped lanthanum manganite .....	786
APPENDIX: EXPERIMENTAL TECHNIQUE AND STRUCTURES UNDER STUDY .....	788
A.1. Experimental set-ups .....	788
A.2. Models of 1D photonic crystals and left handed metamaterials .....	789
References .....	790

## 1. INTRODUCTION

In recent years the attention of researchers is attracted to the study of metamaterials, i.e. such materials, which features are defined not so much by the properties of natural materials components forming them, but first of all by the spatial arrangement of these components. Namely, the possibility of effective control of the electromagnetic waves propagation by means of such special artificial media (metamaterials, composite media) is one of the most interesting fundamental questions here. This interest revealed itself primarily by the large exponentially growing literature (articles and monographs) on this question. Without the task of detailed survey of the literature, we mention here only a few recent monograph and reviews in which it is possible to find a detailed bibliography on the theme [1–3].

The most interesting and paradoxical representatives of the abovementioned media which will be addressed in this review are the photonic/magnetophotonic crystals and left-handed media.

Photonic crystals (PC), whose intensive study began in 1987 (E. Yablonovich and S. John) are structures with spatial periodicity of the dielectric constant. The periodicity has the order of optical wavelengths. These structures are very attractive to control the transmission of light. Using a photonic crystal, the photon can be manipulated in various ways: it is possible to make a channel within the crystal, from which light can not go outside, it is possible to make a cavity inside the crystal and confine the light it in, and finally it is possible to get a slow light with very small group velocity. The basis for all these phenomena is a special, zonal/band structure of radiation in the crystal which is caused by the periodicity of its properties and which is principally different from the uniform material. All these special features of propagation led not only to discovery of many new physical effects, but also became the base of many devices.

If a material of PC is magnetic or even if the only defect of its structure is magnetic the resulting magnetophotonic crystal (MPC) manifests unique optical and magneto-optical properties, in particular, for example, a sharp increase in the Faraday effect due to the smallness of the speed of light. In addition, it is possible to control the band structure of the crystal with the applied external magnetic field.

It is very important that the special features remain also true in microwave range, and moreover some of them they become even more pronounced.

The second class of substances, which was mentioned above, the left-handed media are also potential for a variety of physical effects and the possibility of their practical implementation. Associate with the name of Veselago (1967), these media attract researchers with the ability to create superlens, superprism and a number of other devices.

Note that the left-handed media are geometrically scalable and their properties can be realized in a wide range of operating frequencies including radio, microwave, millimeter wave, and up to visible light band. Recently an acoustic analogue of electromagnetic metamaterials the so-called ultrasonic metamaterials was demonstrated.

The purpose of this review is the study of the properties of the artificial media created on the basis of semiconductors, ferrites, wire media for microwaves. Primary attention in this case is paid to the examination of the effects connected with the violation of periodicity of the structures. At the same time, the properties of natural left medium on the basis of the manganite of lanthanum with the structure of perovskite are also discussed.

This review presents the results of experimental and theoretical study of the transmission of microwave radiation through the composite media; further study of such media can be the basis of new microwave technology. The review also discusses physics of artificial materials (metamaterials), which are formed by the natural elements/materials of two kinds. The first ones are “carriers of permittivity” and are presented by plasma-like media and semiconductors. The second ones are “carriers of permeability” — they are presented by ferromagnets. Among such ferromagnets are ferroelectrics (ferrites) and manganite-perovskite compounds.

In the first chapter of the review various aspects of the electrodynamics of periodical structures — magnetophotonic crystals — are considered. Experimental results are presented describing the interaction of radiation with such periodical structures, the appearance of zone structure of levels and its modification for possible violations of periodicity (Tamm states, defect mode) as well as the influence of external magnetic field on the spectral characteristics of magnetophotonic crystals.

The second chapter of the review is devoted to the electrodynamics of so-called left-handed media (media with negative permittivity and permeability). Different versions of composite left-handed media and refraction characteristics in them are considered. It is shown that one of effective experimental methods of detecting the left-handed properties are the change of refraction in prism and use of T-junction waveguide. Particular attention is paid to features of electrodynamics of synthesized natural left-handed media. In this case we have in mind doped lanthanum manganites, which in a certain concentrations of doping element and temperature range are conducting ferromagnets and can serve as an example of natural left-handed media.

The Appendix describes the details of experimental techniques.

Note that the special emphasis should have the research and design of the listed above metamaterials in a range of low temperatures. This is due to the fact that a main disadvantage of artificial materials under study (quite large losses, i.e. quite small relaxation times) becomes less noticeable with the temperature decreasing. At the same time the main advantage (namely the possibility to control their frequency dispersion, spectra zone structure) remains. Thus the most prospective areas of application of the magnetic metamaterials lie probably at low temperatures.

## 2. PHOTONIC CRYSTALS, EFFECTS OF INHOMOGENEITY

In this chapter various aspects of propagation of microwave radiation in the so-called photonic/magnetophotonic crystals (PC/MPC) are considered.

Photonic crystals are characterized by a special type of interaction with electromagnetic radiation. This interaction is a consequence of the discrete translational symmetry of these crystals. Namely, their electromagnetic properties (characteristic parameters of the medium) are periodic with respect to certain discrete group of translations. This leads to appearance of allowed and forbidden bands/zones for the transmission of the radiation through the PC, in complete analogy with process of electron wave propagation in the crystal lattice.

Although in the case of PC, we are faced with a number of significant differences (quanta of light in contrast to the electrons do not interact with each other, and Maxwell equations in contrast to the Schrödinger equation are the equations for vector fields), electromagnetic waves in the PC are described with Bloch functions. Therefore a number of allowed and forbidden levels/zones, as well as *special states appear in the forbidden zone of the crystal*. They are the so-called *surface states* associated with the boundary, and the so-called *defect modes* associated with the violation of translational periodicity.

Magnetophotonic crystals is characterized by the presence of magnetic elements (e.g., ferrite) in the unit cell, so

their properties depend on the external applied magnetic field. The microwave band is very favorable for studying the properties of MPC, since at more high, optical frequencies, the effect of magnetic field on the magnetic and dielectric constant is extremely small.

A quite comprehensive theoretical analysis of different types of surface states is given in [4,5]. In particular, it was shown that at the boundary of the PC (with a medium with negative permittivity, as well as at the boundary between the two photonic crystals), the uniform solutions along the interface can exist (which do not carry energy, i.e.,  $k_x=0$ ). These solutions are so-called *electrodynamic Tamm surface states* (TS).

Ideal TS is formed in infinite structures at the boundary of two semi-infinite photonic crystals. In finite structures, we deal with in a real experiment, the TS leads to resonant tunneling of microwave radiation through the structure and manifests itself as a transparency peak in the transmission spectrum at the frequency of TS. Experimentally the TS can be detected by measuring the transmission coefficient for wave propagating through the layer of PC with finite thickness, adjoin a layer of material with  $\epsilon < 0$ . Note that the dependence of TS position on  $\epsilon$ , in principle, makes it possible the experimental measurement of this quantity.

The frequency of TS on the boundary between two photonic crystals is defined by equality of input impedances. These quantities are evaluated at  $k_x = 0$ . The Bloch wave numbers for both media must be complex and waves should decrease in the direction away off the interface. Note that the input impedances are entirely determined by the structure of the PC unit cell. However, they differ from the average characteristic impedance of the cell. Besides, the input impedance depends on the direction of wave propagation, so we need to distinguish between “left” and “right” input impedances.

In conclusion, we have point out one important property of the PC. The collective excitations in PC are described by the new wave vector — the Bloch vector, which is determined by the periodicity of the material properties. If the wave vector of electromagnetic wave becomes imaginary in one of the layers, as it is in the case of the semiconductor, the field in this layer decreases exponentially in the direction away off the boundary. In a homogeneous substance such condition implies a non-transmission of waves. But in a periodic medium, the propagation of waves is allowable, even if the total internal reflection takes place in one of the layers [6].

### 2.1. Magnetically controllable 1D magnetophotonic crystal

In this section a simple theoretical phenomenological model of 1D ferrite-based magnetophotonic crystal in millimeter waveband is developed [7]. The possibility to con-

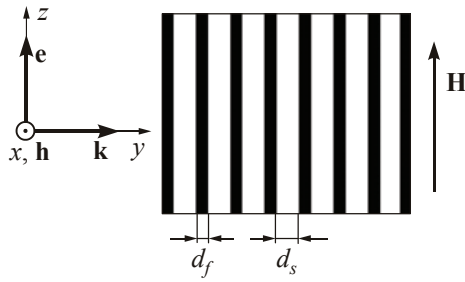


Fig. 1. The structure under consideration ( $\mathbf{h}$ ,  $\mathbf{e}$  are the magnetic and dielectric components of the ac field,  $\mathbf{H}$  is the static magnetic field).

ontrol spectral properties of such crystal with small external magnetic field is demonstrated experimentally.

### 2.1.1. Phenomenological model of 1D magnetophotonic crystal

The structure under consideration is formed by  $N$  parallel ferrite layers  $d_f$ , separated by the space gaps with the thickness  $d_s$  (Fig. 1). The layers are unrestricted in the  $x$ - and  $z$ -directions. The plane electromagnetic wave with circular frequency  $\omega$  and wave vector  $\mathbf{k}$  falls normally on such structure. The static magnetic field  $\mathbf{H}$  is directed parallel to the layers.

### 2.1.2. Constitutive parameters of ferrite

When the external magnetic field equals zero properties of ferrite are isotropic. Its permittivity and permeability are scalars, and  $5 \leq \epsilon_f \leq 16$ . The magnetized ferrite media is gyrotropic and its permeability is the tensor of the second rank:

$$\hat{\mu} = \begin{bmatrix} \mu & i\mu_a & 0 \\ -i\mu_a & \mu & 0 \\ 0 & 0 & \mu_Z \end{bmatrix}. \quad (2.1)$$

The permittivity in this case is a scalar [8]. It is known that components of this tensor can be represented as solutions of the equation of motion of magnetization [9]. For saturated ferromagnet we have

$$\mu = \frac{\omega_H (\omega_H + \omega_M) - \omega^2}{\omega_H^2 - \omega^2}, \quad \mu_a = \frac{\omega_M \omega}{\omega_H^2 - \omega^2}, \quad (2.2)$$

where  $\omega_H = \gamma H$ ;  $\omega_M = \gamma 4\pi M_S$ ;  $\omega = 2\pi f$  is the circular frequency of the alternating electromagnetic field,  $H$  is the external static magnetic field,  $M_S$  is the saturation magnetization of a ferromagnet,  $\gamma$  is the gyromagnetic ratio. The magnitude  $\mu_Z$  is close to unit and does not depend on external magnetic field.

Below we apply some phenomenological approach and describe the properties of non-saturated ferrites by empirical expression (for instance [10–12]), which is in a good agreement with experiment. We used the permeability of absolutely demagnetized ferrite, calculated on the ground of a two-domain model [13]:

$$\mu_{\text{dem}} = \frac{1}{3} + \frac{2}{3} \sqrt{1 - \left( \frac{\gamma M_S}{\omega} \right)^2}. \quad (2.3)$$

This relation describes the experiment quite satisfactorily. For diagonal tensor components  $\mu$  and  $\mu_Z$  of non-saturated ferrite we use the expression [14]:

$$\mu = \mu_{\text{dem}} + (1 - \mu_{\text{dem}}) \left( \frac{M(H)}{M_S} \right)^{3/2}, \quad (2.4)$$

$$\mu_Z = \mu_{\text{dem}} \left[ (1 - M(H)/M_S)^{5/2} \right], \quad (2.5)$$

where  $\mu_{\text{dem}}$  is the permeability of absolutely demagnetized ferrite, defined by (2.3);  $M(H)$  is the magnitude of the technical magnetization. The dependence  $M(H)$  is defined by the experimental way.

Nondiagonal components are defined by the expression (e.g. [8])

$$\mu_a = -4\pi \frac{\gamma M}{\omega}, \quad (2.6)$$

obtained by averaging over domains the solutions of magnetization equations of motion.

### 2.1.3. The propagation of a plane wave through the ferrite

Now using (2.4)–(2.6) we consider the propagation of a plane wave through the ferrite. It is known that Maxwell equations in gyrotropic media [9] have two solutions, which correspond to two normal modes. Each mode has its own propagation constant

$$k_{1,2} = k_0 \sqrt{\epsilon \mu_{\text{eff1}, \text{eff2}}}, \quad (2.7)$$

where  $k_0 = \omega/c$  is the propagation constant in ambient space,  $c$  is the velocity of light.

The first mode is “the ordinary mode”, for which the vector magnetic component is directed parallel to the static magnetic field ( $\mathbf{h} \parallel \mathbf{H}$ ). This mode has the effective permeability

$$\mu_{\text{eff1}} = \mu_Z. \quad (2.8)$$

The second one is the “extraordinary mode” with  $\mathbf{h} \perp \mathbf{H}$ , and effective permeability

$$\mu_{\text{eff2}} = \frac{\mu^2 - \mu_a^2}{\mu}. \quad (2.9)$$

Figure 2 shows the  $\mu_{\text{eff1}}$ ,  $\mu_{\text{eff2}}$  for the high-frequency ferrite (brand 1SCH4).

These dependencies are defined by (2.4)–(2.6) for explicitly non-saturated case ( $H < 1$  kOe) and by (2.2) for explicitly saturated case ( $H > 1.8$  kOe). The dashed line in the figure corresponds to the values where the ferrite transforms from non-saturated into saturated state. The above-mentioned models do not describe the permeability correctly. It is easy to see from the Fig. 2 that  $\mu_{\text{eff2}}$  varies with magnetic field more steeply than  $\mu_{\text{eff1}}$ . Therefore, the ex-

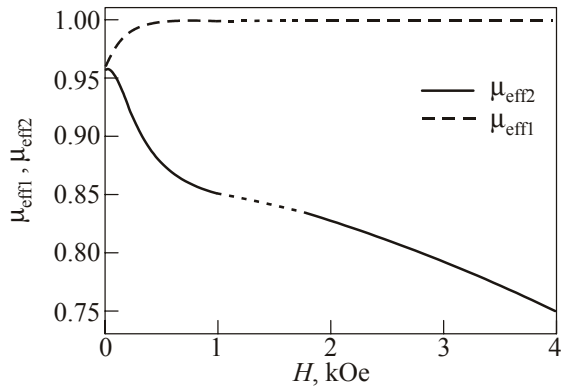


Fig. 2. Effective permeability of ferrite (brand 1SCH4,  $M_S = 4800$  G) versus static magnetic field for the ordinary mode ( $\mathbf{h} \parallel \mathbf{H}$ ) and for the extraordinary mode ( $\mathbf{h} \perp \mathbf{H}$ ) at  $f = 39$  GHz.

traordinary mode is more preferable in order to control the magnetophotonic crystal spectrum.

2.1.4. Transmission spectra of the multilayered periodical structure

We use the known transfer matrix technique [15] to find the transmission coefficient for the multilayered periodical structure (Fig. 1). The magnitudes of tangential components of electromagnetic field are connected by the  $2 \times 2$  matrix  $\hat{T}$ :

$$\begin{bmatrix} e_t(z_2) \\ h_t(z_2) \end{bmatrix} = \hat{T}(z_2, z_1) \begin{bmatrix} e_t(z_1) \\ h_t(z_1) \end{bmatrix}. \quad (2.10)$$

Due to continuity of tangential components on the boundary between layers the transfer matrix is a unit matrix. The transfer matrix  $\hat{M}$  through the whole structure is a multiplication of matrixes for separate layers  $\hat{T}_i$ :

$$\hat{M} = \prod_{i=1}^N \hat{T}_i. \quad (2.11)$$

We calculated the transmission spectrum of the multilayer periodical structure. The structure consists of eight ferrite plates (C4-type,  $M_S = 4800$  G) with thickness  $d_f = 1$  mm and space gaps thickness  $d_s = 2$  mm. The transmission-zones (pass-bands) and stop-zones (stop-bands) are shown in Fig. 3 at the frequency band 30–85 GHz for the following four cases  $H$ , kOe: 0 and 1 ( $\mathbf{h} \parallel \mathbf{H}$ ); 1 and 3.8 ( $\mathbf{h} \perp \mathbf{H}$ ).

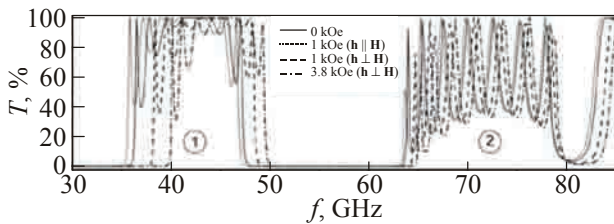


Fig. 3. Shift of stop-bands in the transmission spectra of eight-layered 1D MPC for ordinary and extraordinary waves.

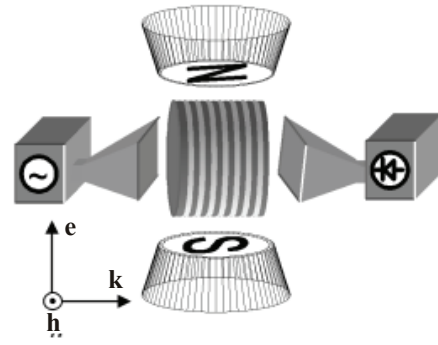


Fig. 4. The scheme of experiment.

It is easy to see that pass-bands have typical rectangular-type shape with some oscillations near edges. It is important to note, that for  $\mathbf{h} \perp \mathbf{H}$  the stop-band shifts to higher frequencies by  $\Delta f \approx 3$  GHz (under changes of the magnetic field 0–3.8 kOe). For  $\mathbf{h} \parallel \mathbf{H}$  the stop-band shifts to lower frequencies by  $\Delta f \approx 0.6$  GHz (under changes of the magnetic field 0–1 kOe). Thereby these graphs demonstrate the possibility of detuning of stop-bands with magnetic field. The steepness of the stop-band edge reaches 0.017 dB/MHz and increases with increasing of the number of layers.

2.1.5. Experiment

To verify the mathematical model, we carried out the experimental study of the periodic structure, consisting of eight ferrite layers with  $D_s = 30$  mm. Space gaps are formed by thin rings with thickness  $d_s = 2$  mm.

The sketch of the experiment is presented in Fig. 4. The plane wave (the frequency band 27–40 GHz) falls on the multilayer, which is located in the magnetic field between 0–4 kOe. Measurements have been carried out for both  $\mathbf{h} \parallel \mathbf{H}$  and  $\mathbf{h} \perp \mathbf{H}$  orientations at room temperature.

In Fig. 5 the theoretical and experimental data show dependencies of stop-band frequency edges on magnetic

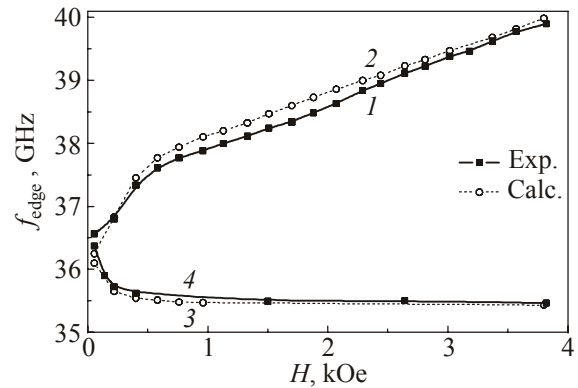


Fig. 5. Frequency of the stop-band edges versus the magnetic field for two waves with the mutually perpendicular polarization: for the ordinary mode (curves 3, 4) and for the extraordinary mode (curves 1, 2).

field. Two waves with mutually perpendicular polarizations: for the ordinary mode (curves 3, 4) and for the extraordinary mode (curves 1, 2) were considered. The experiment and theory are in good agreement in spite of the fact that theoretical description does not take into account any losses in ferrite. Another important detail: the extraordinary wave is more preferable for practical applications because its frequencies are higher (Fig. 5).

**2.2. Defect mode in magnetophotonic crystal with ferrite defect element**

We consider now the influence of the external magnetic field on the spectrum of spatially restricted PC with a defect layer. The defect layer (see Fig. 6) violates the translation symmetry conditions which in turn changes the zone spectrum of the crystal. A new element, defect mode, appears in the crystal spectrum. Note here that the position of the defect mode in the spectrum depends on specific details of PC structure with defect layer and of applied magnetic field (see Sec. 2.3).

To study the defect zone experimentally, we used PC formed by eight alternating polystyrene-air layers, and we have replaced one of layers inside the crystal by “defect” ferrite layer [16].

The plane electromagnetic wave falls on the structure perpendicularly to the plane of layers. The condition  $d_p n_p = d_s n_s \approx \lambda_0/4$ , where  $n_i = \sqrt{\epsilon_i \mu_i}$  holds true for PC layers and  $d_f n_f(H) = \lambda_0/2$  for the “defect” layer ( $\lambda_0$  is the wavelength in vacuum). The calculation by the transfer matrix method proves the occurrence of narrow “defect” mode in the transmission spectrum of the structure. Really the elements of the structure at the left and at the right of the “defect” layer are Bragg-reflectors so the whole structure can be considered as Fabri–Perot resonator, tuned on the first longitudinal mode. The shape of experimentally obtained spectrum of the “defect” mode (Fig. 7) is described satisfactory by the Lorenz function.

The experimental verification supports the conclusions of mathematical model describing the spectrum of the structure with frequency dispersive “defect”. The error for the dependence of the “defect” mode frequency on the applied magnetic field does not exceed 2% between experiment and simulation (Fig. 8).

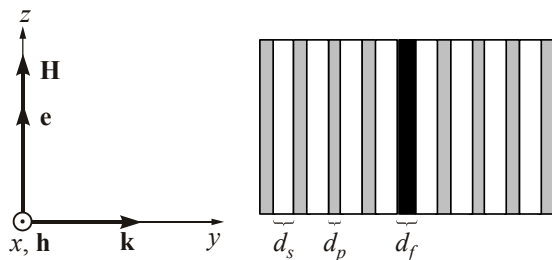


Fig. 6. Scheme of polystyrene-air PC with ferrite “defect” layer.

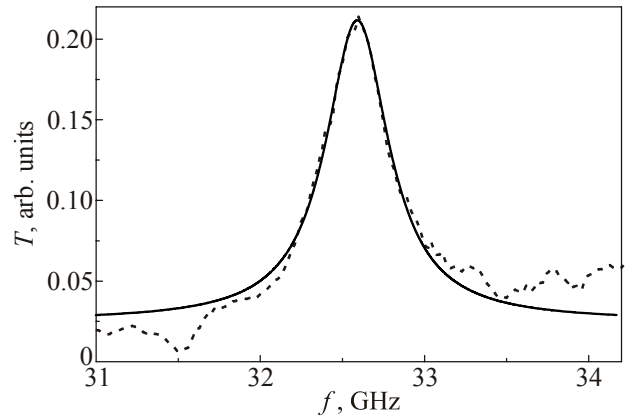


Fig. 7. Experimental spectra of the “defect” mode in the 1D PC with ferrite “defect” layer.

**2.3. Defect mode in magnetophotonic crystal with semiconductor defect element**

In this section properties of another defect structure in the external applied magnetic field are investigated experimentally and theoretically: *the ferrite-dielectric periodic structure with defect semiconductor layer*. It is found, that the position of defect mode in periodic structure depends on the position and of environment of defect layer in periodic structure, i.e., on the boundary conditions. The transmission properties of the structure depends whether the defect semiconductor layer is surrounded with layers of different nature or with layers with similar nature [13].

1D periodic structure is formed from alternating ferrite and dielectric layers of thicknesses  $d_f$  and  $d_d$ , respectively. The thickness of the “defect” semiconductor layer is  $d_s$ . Here and further parameters with indexes  $d, f$  and  $s$  refer to the dielectric, ferrite and semiconductor layer, respectively. The thickness of the structure is  $L = N_L d + d_s + N_R d$  ( $N_L$  and  $N_R$  are the number of periods at the left and right of defect, respectively:  $d = d_f + d_d$  is the period of the structure). The structure is

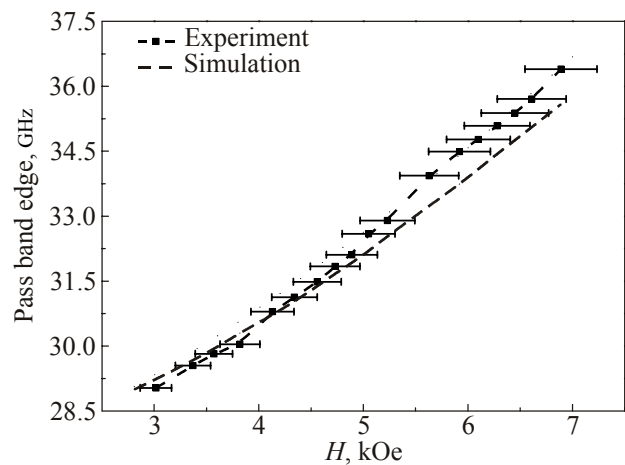


Fig. 8. “Defect” mode frequency on the applied magnetic field for 1D PC.

placed between two semiinfinite homogeneous media with dielectric permittivities  $\epsilon_a$  and  $\epsilon_b$ . The structure is uniform in  $y$  direction. ( $x$  axis is parallel to the boundaries of the layers and the  $z$  axis is perpendicular to the layers. The incident, reflected and transmitted wave vectors lie in the  $xz$  plane. The magnetic field is directed along  $y$  axis.)

Theoretical analysis of such a structure has been carried out using the Maxwell equations for each layer of the considered structure with corresponding boundary conditions (the continuity of the tangential components of the electric and magnetic fields on all boundaries). The Maxwell equations split into two independent systems for TM and TE polarization and we consider later only TE waves ( $H_x, E_y, H_z \neq 0$ ).

The permeability of the ferrite layer has a usual form [17] and its permittivity tensor is diagonal  $\epsilon_{ii} = \epsilon_f$ . Components of the semiconductor permittivity tensor are:

$$\begin{aligned} \epsilon_{\parallel} = \epsilon_{xx} = \epsilon_{zz} = \epsilon_0 \left( 1 - \frac{\omega_p^2 (\omega + i\nu)^2}{\omega \left[ (\omega + i\nu)^2 - \omega_c^2 \right]} \right), \\ \epsilon_{\perp} = \epsilon_{xz} = -\epsilon_{zx} = \epsilon_0 \frac{i\omega_c \omega_p^2}{\omega \left[ (\omega + i\nu)^2 - \omega_c^2 \right]}, \quad (2.12) \\ \epsilon_{yy} = \epsilon_0 \left( 1 - \frac{\omega_p^2}{\omega (\omega + i\nu)} \right). \end{aligned}$$

Here  $\omega_p$  and  $\omega_c$  are the plasma and cyclotron frequencies, correspondingly,  $\epsilon_0$  is the lattice permittivity,  $n$  is the carrier concentration,  $\nu$  is the collision frequency;  $\mu_{ii} = 1$ .

To satisfy the boundary condition in the case periodic structure we use the transfer matrix method [6,15].

$$\begin{pmatrix} E_y(0) \\ H_x(0) \end{pmatrix} = \hat{m} \begin{pmatrix} E_y(d) \\ H_x(d) \end{pmatrix}. \quad (2.13)$$

The finiteness of the periodic medium is taken into account by the Abeles theorem [6,15] by means of which we raise the transformation matrix  $\hat{p} = \hat{m}_f \cdot \hat{m}_d$  for elementary cell of the periodic structure to the  $N$ th power  $\hat{S}_{L,R} = (\hat{p}_{L,R})^N$ .

The transmission coefficient can be presented as:

$$T = \frac{2 \frac{c}{\omega} k_{za} \exp(-ik_{zb}L)}{\frac{c}{\omega} k_{za} m_{11} - \left( \frac{c}{\omega} \right)^2 k_{za} k_{zb} m_{12} + m_{21} + \frac{c}{\omega} k_{zb} m_{22}}. \quad (2.14)$$

Here  $m_{ik}$  are the components of the transformation matrix  $\hat{m} = \hat{S}_L \cdot \hat{m}^s \cdot \hat{S}_R$ .

### Experiment

The details of the structure and the experimental technique are presented in [13,18]. The quartz layer permittivity is  $\epsilon_d = 4.5$ . The ferrite layer has complex permittivity of

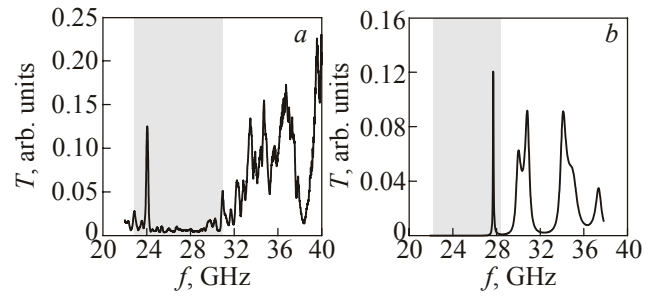


Fig. 9. Experimental (a) and theoretical (b) spectra. Neighboring layer at the left of the defect layer is dielectric, and at the right is ferrite,  $H_0 = 2$  kOe. Defect mode appeared in the forbidden zone (shaded).

about  $\epsilon_2 = 11.1 + 0.0008i$ , with saturation magnetization  $4\pi M_S = 4800$  G and damping coefficient  $\alpha = 0.024$ . The semiconductor (InSb) has the following parameters: lattice permittivity  $\epsilon_0 = 17.8$ , carrier concentration  $n = 2 \cdot 10^{14} \text{ cm}^{-3}$  (at 77 K), collision frequency  $\nu = 2 \cdot 10^{11} \text{ s}^{-1}$ .

The transmission properties were studied in the frequency range where the forbidden zone of the periodic structure coincides with semiconductor layer negative permittivity region. It was found that if the defect semiconductor layer is surrounded with different layers, then the considered structure becomes a “the nonreciprocal system”: the transmission properties of the considered structure are changed if the direction of electromagnetic wave propagation is changed (i.e. if the wave falls from the medium  $b$ ) (Figs. 9 and 10; the forbidden zone is shaded). On the contrary, if the defect layer is surrounded with similar layers then such a structure is “the reciprocal system”.

The influence of the external magnetic field on the transmission properties of the structure investigated. The transmission peak shifts to the higher frequencies with increasing of external magnetic field (Fig. 11). As properties of the semiconductor layer are independent on the magnetic field ( $\mathbf{H}_0$  is perpendicular to the vector of magnetic component of the field); the peak shift is connected with magnetic field dependence of ferrite permeability. Intensity of the transmission peak also changes with increasing of external magnetic field.

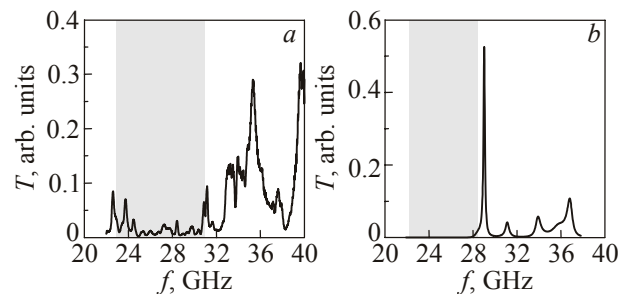


Fig. 10. Experimental (a) and theoretical (b) spectra. Neighbouring layer at the left of the defect layer is ferrite, and at the right is dielectric,  $H_0 = 2$  kOe. No defect mode appeared in the forbidden zone.

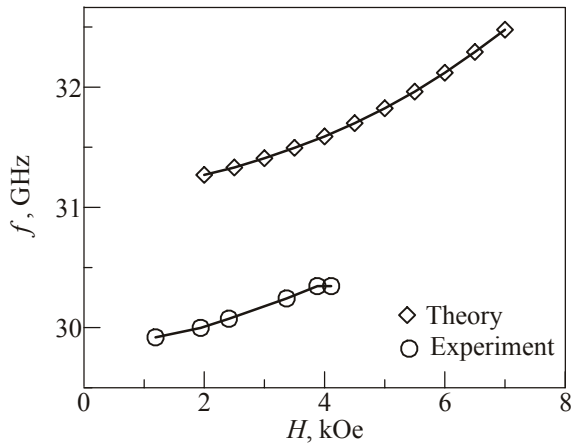


Fig. 11. Dependence of the “defect” peak frequency on the external magnetic field.

It should be noted, that experimental and theoretical results agree qualitatively and some difference between these results is caused by shortcomings of the theoretical model.

#### 2.4. Tamm states in magnetophotonic crystals and permittivity of the wire medium

In this section a system consisting of magnetophotonic crystal and a negative permittivity medium (NPM) was studied both experimentally and theoretically in the microwave frequency band [18]. The NPM was prepared as a set of conductive wires (wire medium, WM). The three-layer elementary cell of MPC comprised of air, ferrite and quartz layers. A change of TS spectral position was calculated theoretically for two cases: depending on thickness of air layer in the MPC elementary cell and on the value of NPM negative permittivity. Using the experimental frequency position of the TS we solved the inverse problem and found effective permittivity of the medium bounding the MPC. Therefore a method of measuring the value of medium effective permittivity on the base of TS frequency position was proposed.

The specimen under study (Fig. 12) represents 1D MPC placed into the section of single-mode waveguide  $7.2 \times 3.4$  mm. The structure consisting of the sequence (4 cells) of three-layer elementary cells is in contact with a

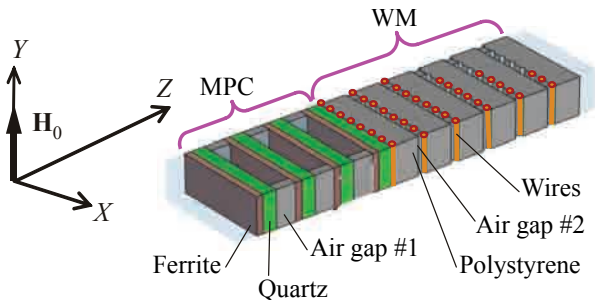


Fig. 12. Scheme of the structure under study.

wire medium WM. The WM is a set of thin wires on polystyrene substrate, the distance between wires is much less than the waveguide wavelength.

The studied structure is placed in a gap of the electromagnet, the static magnetic field  $\mathbf{H}_0$  being perpendicular both to the wave vector (along  $z$  axis) and the vector of magnetic component of the wave (along  $x$  axis). With this field configuration the extraordinary wave propagates in ferrite. The wave transmission coefficient was measured in the frequency band of 22–40 GHz.

##### 2.4.1. TS equations

To derive the equation for Bloch wave number we consider TE wave propagating along the axis of the periodical structure and use the method of  $2 \times 2$  transition matrix (see for example [5,6]). Fourier components  $E_y$  and  $H_x$  in the  $i$ th layer ( $i = 1, 2, 3$ ) are related by

$$H_x = \frac{j c}{\mu_i \omega} \frac{\partial}{\partial z} E_y = -\zeta_i E_y, \quad (2.15)$$

where

$$E_y = A_i \exp(jk_{zi}(z - z_i)) + B_i \exp(-jk_{zi}(z - z_i))$$

and

$$\zeta_i = \frac{k_{zi} c}{\mu_i \omega}, \quad k_{zi} = \sqrt{\varepsilon_i \mu_i \frac{\omega^2}{c^2} - k_x^2}.$$

(Due to uniformity in  $x$  the  $x$ -dependence is proportional to  $\exp(jk_x x)$  with constant  $k_x$ .)

The transfer matrix  $\hat{M}$  for elementary cell is product of the layers transition matrices and for three-layer cell the corresponding unimodular matrix  $\hat{M}$  has the form:

$$\hat{M} = \begin{pmatrix} m_{11} & m_{12} \\ m_{21} & m_{22} \end{pmatrix}, \quad (2.16)$$

where the matrix components  $m_{ik}$  are

$$\begin{aligned} m_{11} &= \cos \alpha_3 \cos \alpha_2 \cos \alpha_1 - \frac{\zeta_1}{\zeta_2} \cos \alpha_3 \sin \alpha_2 \sin \alpha_1 - \\ &- \frac{\zeta_2}{\zeta_3} \sin \alpha_3 \sin \alpha_2 \cos \alpha_1 - \frac{\zeta_1}{\zeta_3} \sin \alpha_3 \cos \alpha_2 \sin \alpha_1, \\ m_{12} &= -\frac{i}{\zeta_1} \cos \alpha_3 \cos \alpha_2 \sin \alpha_1 - \frac{i}{\zeta_2} \cos \alpha_3 \sin \alpha_2 \cos \alpha_1 + \\ &+ \frac{i\zeta_2}{\zeta_1 \zeta_3} \sin \alpha_3 \sin \alpha_2 \sin \alpha_1 - \frac{i}{\zeta_2} \sin \alpha_3 \cos \alpha_2 \cos \alpha_1, \\ m_{21} &= -i\zeta_3 \sin \alpha_3 \cos \alpha_2 \cos \alpha_1 + \frac{i\zeta_3 \zeta_1}{\zeta_2} \sin \alpha_3 \sin \alpha_2 \sin \alpha_1 - \\ &- i\zeta_2 \cos \alpha_3 \sin \alpha_2 \cos \alpha_1 - i\zeta_1 \cos \alpha_3 \cos \alpha_2 \sin \alpha_1, \\ m_{22} &= -\frac{\zeta_3}{\zeta_1} \sin \alpha_3 \cos \alpha_2 \sin \alpha_1 - \frac{\zeta_3}{\zeta_2} \sin \alpha_3 \sin \alpha_2 \cos \alpha_1 - \\ &- \frac{\zeta_2}{\zeta_1} \cos \alpha_3 \sin \alpha_2 \sin \alpha_1 + \cos \alpha_3 \cos \alpha_2 \cos \alpha_1, \end{aligned} \quad (2.17)$$

where  $\alpha_i = k_{zi}d_i$ , here index  $i$  ( $i = 1, 2, 3$ ) is number of the layer.

Floquet's theorem accounts the periodicity of the MPC:

$$\hat{M} \begin{pmatrix} E_y(0) \\ H_x(0) \end{pmatrix} = e^{ik_B d} \begin{pmatrix} E_y(0) \\ H_x(0) \end{pmatrix}, \quad (2.18)$$

where  $k_B$  is a Bloch wave number and  $d = d_1 + d_2 + d_3$  is the period of MPC. Using equation (2.17) and relations (2.18) we obtain the dispersion equation for Bloch wave number in the form

$$\begin{aligned} \cos k_B d &= \cos \alpha_3 \cos \alpha_2 \cos \alpha_1 - \\ &- \frac{1}{2} \left( \frac{\zeta_1}{\zeta_2} + \frac{\zeta_2}{\zeta_1} \right) \cos \alpha_3 \sin \alpha_2 \sin \alpha_1 - \\ &- \frac{1}{2} \left( \frac{\zeta_1}{\zeta_3} + \frac{\zeta_3}{\zeta_1} \right) \sin \alpha_3 \cos \alpha_2 \sin \alpha_1 - \\ &- \frac{1}{2} \left( \frac{\zeta_2}{\zeta_3} + \frac{\zeta_3}{\zeta_2} \right) \sin \alpha_3 \sin \alpha_2 \cos \alpha_1. \end{aligned} \quad (2.19)$$

The dispersion equation for TS follows from the equality of MPC ( $Z = -H_x(0)/E_y(0)$ ) and bounding medium ( $-\sqrt{\epsilon/\mu}$ ) impedances [5], namely

$$\sqrt{\frac{\epsilon}{\mu}} = \frac{m_{21} - \zeta_2(m_{11} - e^{jk_B d})}{m_{22} - e^{jk_B d} - \zeta_2 m_{12}} \Big|_{k_x=0}, \quad (2.20)$$

where components  $m_{ik}$  are given with the expressions (2.17). The essential feature of TS lies in the fact that component  $k_x$  is zero. This implies that TS is not connected with energy transfer along the interface (MPC-WM). So we should put  $k_x = 0$  in expressions (2.17) for  $m_{ik}$  which enter in the equation (2.20) in the form

$$\alpha_i \Big|_{k_x=0} = \frac{\omega}{c} d_i \sqrt{\epsilon_i \mu_i}, \quad \zeta_i \Big|_{k_x=0} = \frac{c}{\omega} \sqrt{\frac{\epsilon_i}{\mu_i}}. \quad (2.21)$$

The equation (2.20) determines TS frequency, which depends both on internal MPC parameters (thicknesses of layers, permittivities and permeabilities of layers) and the external parameters such as applied magnetic field, permittivity and permeability of the WM. Therefore if TS frequency given, we can determine some of these parameters, in particular permittivity of a finite WM layer. This characteristic can be important if we consider photonic crystal which includes layers with negative permittivity.

#### 2.4.2. Experiment

The typical experimental spectra, namely the transmission coefficient  $T$  through the system (MPC+WM) is presented in Fig 13. The Tamm peak (corresponding to the TS) appears in the forbidden band of the MPC. For the given parameters of the structure its frequency is  $f_{TS} = 24.030$  GHz.  $Q$  factor is about  $10^3$ , that is rather high magnitude for oscillations excited in the waveguide.

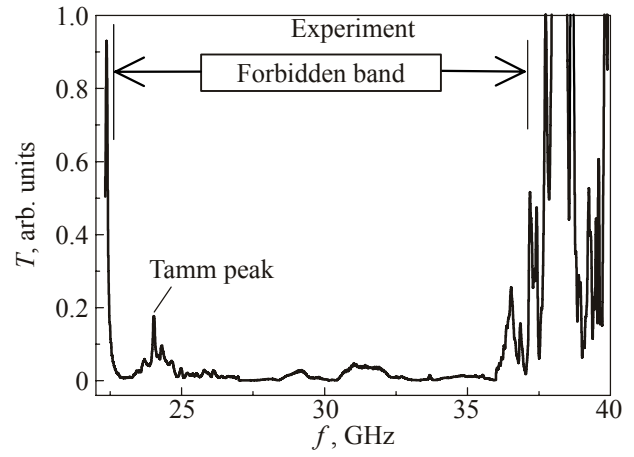


Fig. 13. Experimental spectrum demonstrating the formation of the Tamm peak in the forbidden zone of the MPC for  $H_0 = 1880$  Oe.

With the help of the measured experimental TS frequency we can solve the inverse problem and find the value of WM permittivity. This value equals in this case to  $\epsilon_{WM} = -2.77$ . Using this value of WM permittivity we can solve the Eq. (2.20) and find the change of the TS frequency position depending on the change, for example, of the air layer thickness [18,19].

The experimental TS frequency  $f_{TS}$  position gives the answer to the question about the magnitude of permittivity  $\epsilon_{WM}$  for a finite WM layer. According to our findings (Fig. 14) WM permittivity equals  $\epsilon_{WM} = -2.77$ . Therefore the formula overestimates permittivity of WM for given frequency of TS ( $\epsilon_{WM} = -4.68$ ) for host medium — polystyrene.

#### 2.5. Tamm states on the interface of two photonic crystals

In this section TS appeared in 20–40 GHz band on the interface of adjoining 30 mm disk-shaped photonic crystals [20,21] (Fig. 15) is considered. The first is MPC and it

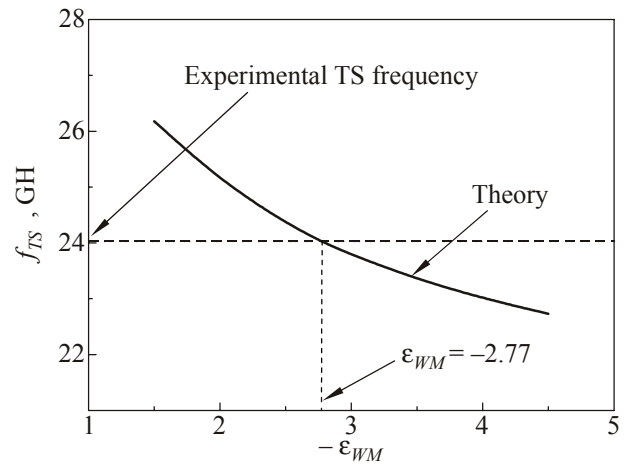


Fig. 14. Variation of the TS frequency with the change of the WM permittivity  $\epsilon_{WM}$  for magnetic field  $H_0 = 1880$  Oe at  $d_{a1} = 1.5$  mm.

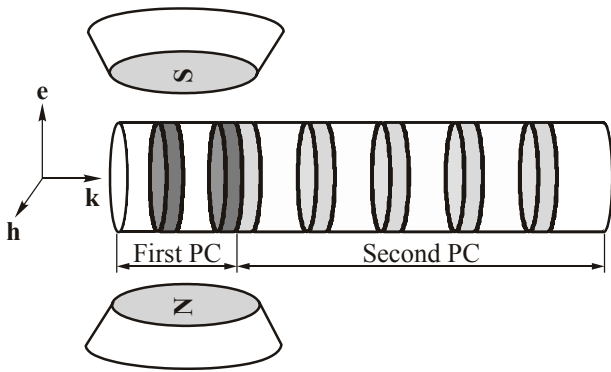


Fig. 15. The scheme of experiment.

consists of two periods of ferrite/air. The second is PC and it consists of five periods of polystyrene/air.

The structure under consideration is placed inside absorbing cylinder and was fixed inside the air-gap of the electromagnet. The external magnetic field is parallel to polarization of incident wave (Fig. 15).

### Results and discussion

In the absence of the external field (zero magnetization) one can see the peak in transmission spectra (Fig. 16). This peak appears only for adjoining structure of two-photonic crystals and does not exist for each of them separately. According to calculations the frequency of this peak is the TS frequency  $f_{TS}$ . Although the TS frequency prediction is in good agreement with experiment, this can not be said about peak amplitude. The disagreement is connected with diffraction, due to the finite diameters of the disks and to finite aperture of the incident wave. Theoretical calculations were made by T-matrix method and did not take the diffraction into account.

The TS frequency  $f_{TS}$  increases monotonically with external magnetic field (Fig. 17). This is due to known dependence of magnetic permeability on external magnetic field.

For theoretical evaluation of the field dependence  $f_{TS}(H_{ex})$ , we as above used the experimental tensor of

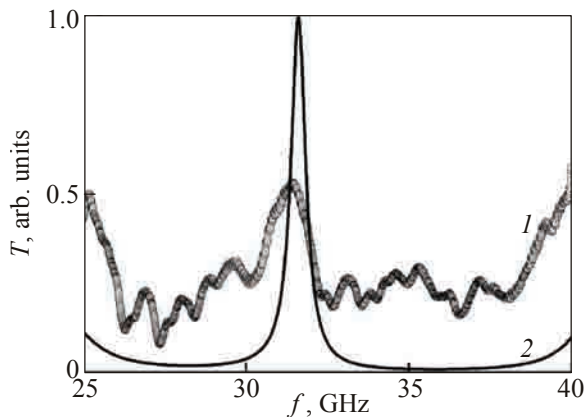


Fig. 16. The transmission of adjoining photonic crystals at zero magnetization: experimental data (1); the theoretical evaluation (2).

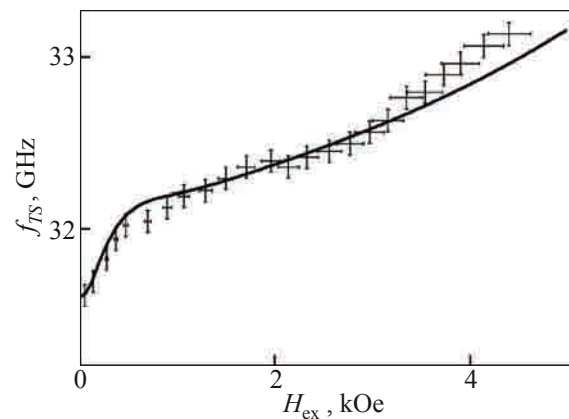


Fig. 17. The dependence of Tamm state frequency  $f_{TS}$  on external magnetic field  $H_{ex}$ .

magnetic permeability at  $H_{ex} \leq 1$  kOe [7] and the well-known expressions at  $H_{ex} \geq 1$  kOe [9]. According to Fig. 17 a good agreement exists between theoretical and experimental data.

### 2.6. Tamm states on the interface of magnetophotonic crystal and semiconductor

In this section peculiarities of the transmission spectra of the MPC interfaced with semiconductor layer are studied experimentally and theoretically [22]. The TE and TM polarizations are considered: Elementary cell of the MPC consists of the air, ferrite and quartz layers.

#### Experiment

The MPC consists of 4 three-layered cells (see details in [22]). The semiconductor (InSb) adjoining the MPC quartz layer has the following parameters: lattice permittivity is  $\epsilon_0 = 17.8$ , carrier concentration is  $n = 2 \cdot 10^{14} \text{ cm}^{-3}$  (at 77 K), collision frequency is  $\nu = 2 \cdot 10^{11} \text{ s}^{-1}$ . The transmission coefficient was measured at the 22–40 GHz frequency range.

In the frequency range, where the forbidden zone of MPC overlaps with negative permittivity region of the semiconductor layer, the peak of the surface wave was registered. The results of experimental and theoretical investigations of surface states for TE and TM polarizations are presented in Fig. 18. We see that for TE waves the transmission peak (Tamm peak) shifts with increase of external magnetic field to higher frequencies (Fig. 18,b). Properties of semiconductor layer for TE polarization are not sensitive to external magnetic field; peak shift is determined only by dependence of ferrite permeability on the external magnetic field. For the case of the TM polarization (Fig. 18,c) conversely the peak shifts to the lower frequencies. Really the properties of ferrite layer for TM polarization are not sensitive to external magnetic field and are the same as for the dielectric layer; the peak shift for TM polarization is determined by the dependence of semiconductor permittivity on the external

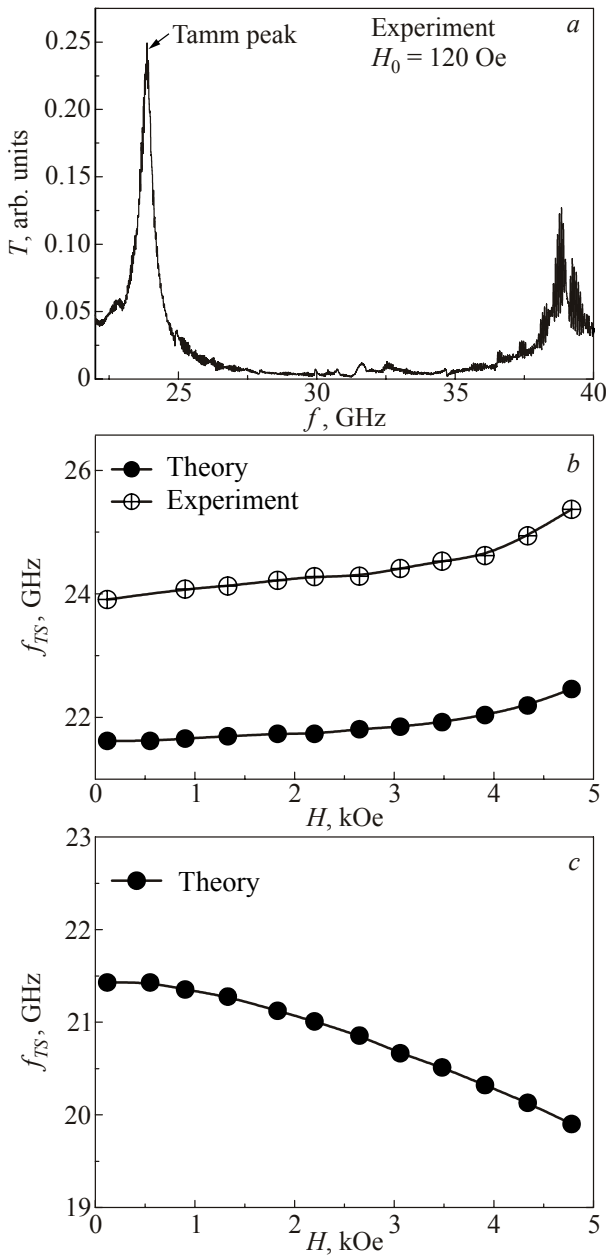


Fig. 18. Tamm peak for the structure under study at  $H_0 = 120$  Oe (a); the shift of Tamm peak frequency on the external magnetic field for the TE polarization (b); for the TE polarization (c).

magnetic field. This difference allows identifying the TE and TM polarizations. Some divergence between the experimental and theoretical results is connected with imperfection of the theoretical model.

**2.7. Peculiarities of the magnetic periodic multilayered ferrite-semiconductor structures**

In this section the results of theoretical and experimental study of transmission spectra of electromagnetic waves for finite periodically layered structure composed of ferrite and semiconductor layers subjected to external magnetic field parallel to the layers are discussed [23]. The

optical thickness of the layers and length of the electromagnetic wave are assumed to be of the same order of magnitude. The wave propagates in Z direction normally to the layers.

The analysis of expression for effective permeability of ferrite layer and dispersion relation obtained for whole (infinite on Z) periodic structure using Floquet theorem [24] reveals three characteristic frequencies: the frequency of ferromagnetic resonance  $\omega_1 = \sqrt{\omega_H(\omega_H + \omega_M)}$  ( $\mu_F \rightarrow 0$ ); the frequency of antiresonance  $\omega_2 = \omega_H + \omega_M$  ( $\mu_{\perp} = 0$ ); from the dispersion equation we obtain the third characteristic frequency  $\omega_3 = \sqrt{\omega_H^2 + \omega_M^2/2 + \omega_H\omega_M}$ . Frequencies  $\omega_1$  and  $\omega_3$  determined the asymptotes of the dispersion curves. Here  $\mu_F = \mu_{\parallel} + \mu_{\perp}^2/\mu_{\parallel}$  is the effective permeability of the ferrite layer.

$$\mu_{\parallel} = \mu_{xx} = \mu_{zz} = 1 + \frac{\omega_M(\omega_H^2 + \omega_r^2 - i\omega_r\omega)}{\omega_H(\omega_H^2 + \omega_r^2 - \omega^2 - 2i\omega_r\omega)}$$

and

$$\mu_{\perp} = \mu_{xz} = -\mu_{zx} = -\frac{i\omega\omega_M}{\omega_H^2 + \omega_r^2 - \omega^2 - 2i\omega_r\omega}$$

are the components of the ferrite layer permeability tensor; where  $\omega_M = 2\pi egM/mc$ ,  $\omega_H = egH_0/2mc$ ;  $g$  is the factor of spectroscopic splitting;  $M$  is the saturation magnetization;  $\omega_r$  is the relaxation frequency.

In Fig. 19 the results of numerical calculation for the case when  $\omega_p < \omega_1$  ( $\omega_p$  is the plasma frequency) are presented. Two main outcomes can be made from these results:

1. In the vicinity of  $\omega_1$  a large amount of allowed bands present. Not difficult to see that the reason of this is a drastic increasing real part of permeability near the ferromagnetic resonance (FMR) frequency.
2. Zones shift to low frequencies and become broader with  $k_x d$  decreasing. Other word, zone should become

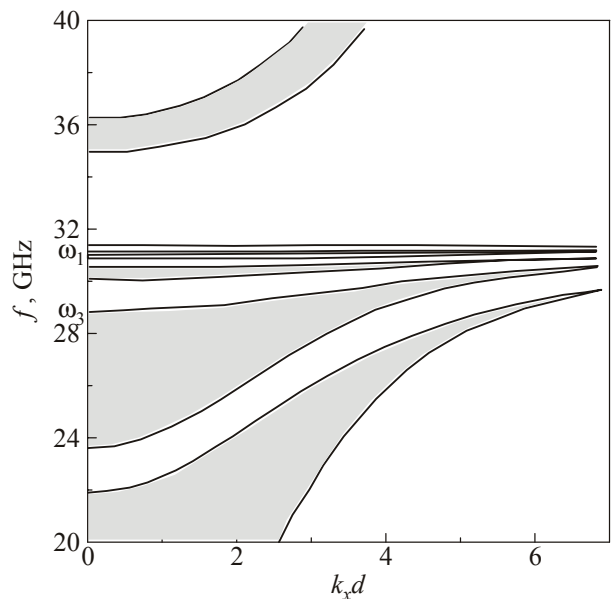


Fig. 19. Dispersion dependence for the infinite structure [23].

broader with decreasing of thickness of all least one of elements, which form such a periodical structure.

Note, that to describe the real structure, i.e. the finite-in-the  $z$ -direction periodic structure ( $N$  elementary cells) one can use the Abeles theory [10] and get the expression for transmission and reflection coefficients. It is naturally that allowed zones transform now into the set of overlapping Wolf-Bragg peaks. The transmission is unity (the system is transparent) if resonant Wolf-Bragg condition is fulfilled:  $N\bar{k}d = \pi q$ ,  $q = 0, \pm 1, \pm 2, \dots$ . As a result we get  $N - 1$  resonant points in each allowed band of the spectrum. But the physical processes and 2 outcomes presented above do not change.

### Experiment

To verify the outcomes of theory the 1D periodical structure (ferrite/semiconductor) was placed into a waveguide and located between poles of an electromagnet. The vector of external magnetic field  $\mathbf{H}_0$  is parallel to plane of the structure layers and  $\mathbf{H}_0$  is directed normally to the magnetic component of alternating field  $\mathbf{H}_x$ .

The structure was assembled of 3 double cells — bilayers: InSb semiconductor/ferrite (see details in [23]).

The experimental results are in good agreement with theoretical calculations. At increasing of the structure length the Wolf-Bragg resonance (WBR) peaks shift to low frequencies as can be seen in Fig. 20. This agrees also with theoretical conclusions (Fig. 19), where the allowed zones shift to the low frequency domain and their width increases as  $k_x d$  decreases. So the assumption that the forbidden zones disappear in limiting case when the ferrite width tends to zero are justified.

## 3. MEDIA WITH NEGATIVE REFRACTION

In this chapter the propagation of microwaves is studied in various left-handed media (media with negative permittivity and permeability  $\epsilon < 0$ ,  $\mu < 0$ ). In the literature the-

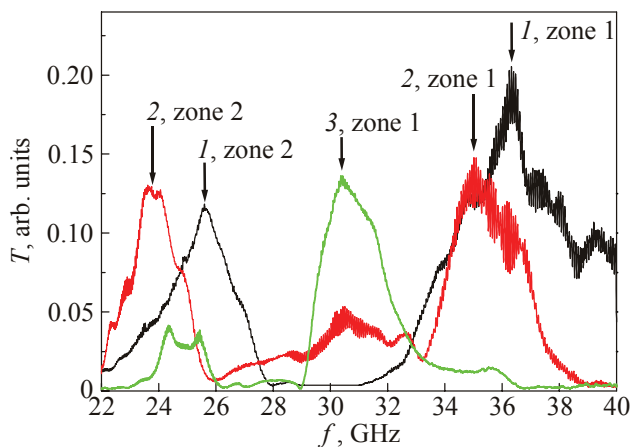


Fig. 20. Transmission spectra for different ferrite layer at different thickness  $d_1$ , mm: 0.5 (1); 1 (2); 1.5 (3), and magnetic field value 5.24 kOe.

se media are known as Veselago media, backward wave media, double-negative media and left-handed media. Although the history associated with the priority of the prediction of this phenomenon is quite complex and confusing (see for example [25]) the important role of Veselago and Pendry is clearly recognized by the international scientific community [26].

The main characteristic features of the propagation of electromagnetic waves in left-handed media are well known to be [27] the appearance of so-called backward wave, anomalous refraction at the interface and the occurrence of anomalous high transparency. We have studied these characteristics experimentally in the case of composite media of different structure and composition. Note that the backward wave has long been well known in the case of inhomogeneous waveguides but the appearance of the backward wave in a homogeneous media, when the direction of phase and group velocities of the wave are opposite, is a clear manifestation of its left properties.

Until recently, the practical realization of left-handed media was accomplished by so-called composites or metamaterials — artificial materials with prescribed electrodynamic properties. As a rule, these materials were tailored of two components: a conductor with a negative permittivity (the role of such conductor played a thin metal layer, a wire medium or semiconductor) and a magnetic subsystem (special magnetic elements, magnetized ferrite). To obtain the effective left media the size of irregularities should be comparable (less than) the wavelength of electromagnetic radiation. In the first subsection of this chapter we consider simulation of metamaterial and appearance of a backward wave when inclusions decrease in size.

Last time [28] a number of natural materials are discovered, which under definite conditions (strong external magnetic field) can have left properties. These materials include doped manganites with perovskite structure. It is known [29] that under certain concentrations of dopant at definite temperature range these substances are conducting ferromagnets; since in the vicinity of FMR their permeability becomes negative, these substances are good candidates as left-handed media [30]. We have studied the behavior of such substances in strong magnetic fields, which led, in particular, to the discovery of the so-called DNG (DNG double negative) states in external fields just above the FMR field.

### 3.1. Formation of backward wave in a metamaterial

Two fundamentally different methods are possible to describe electrodynamic of the composite [12,25,31]. The first method considers the composite medium as consisting of small individual though macroscopic elements and intends to attack the electrodynamic problems (Maxwell equations) for such complex system. This method does not involve the concept of medium effective permittivity and

permeability. The medium is nonuniform: values of permittivity and permeability are different for various elements.

The second method consists in pre-averaging of electrodynamic quantities and in definition of Maxwell equations for this “continuous” medium characterized with averaged effective permittivity and permeability. Naturally the method can be applied when  $\lambda \gg d$ , where  $\lambda$  is a wavelength and  $d$  is characteristic dimension of composite elements. The advantage of this last approach lies in the possibility just to represent the criteria of composite left-handed medium in the form  $\epsilon_{\text{eff}} < 0$ ,  $\mu_{\text{eff}} < 0$ . We stress here that “continuity” of a left-handed medium demands that its permittivity and permeability are negative in the same frequency band and at the same spatial domain.

Properties of two left-handed media were studied and presented here. The first is formed by alternating negative permeability layer (NML) and negative permittivity layer (NEL) and the second correspondingly by metallic wire structure and ferrite plates. The first mentioned above method was used to describe the composite medium: we set electrodynamic parameters of individual elements and

then with the help of computer simulation we considered the propagation of an electromagnetic wave in the 1D metamaterial. Electromagnetic wave pattern visualization was a major advantage of the simulation method. The appearance of a backward electromagnetic wave was an undoubted evidence that initial composite medium can be considered as a left-handed medium with negative effective permittivity and permeability for the wave propagation process. When the dimension of nonuniformity increased the backward wave disappeared and consequently for this electromagnetic process the composite cannot be described as a “continuous” left-handed medium with averaged electromagnetic parameters (effective negative permeability and permittivity).

The composite medium under consideration represents a set of elementary cells, every cell consists of two layers: negative permittivity layer and negative permeability layer. The NML is a ferrite and NEL is a copper wire structure [13,18].

The computer simulation of electromagnetic wave propagating in the one-dimensional metamaterial is pre-

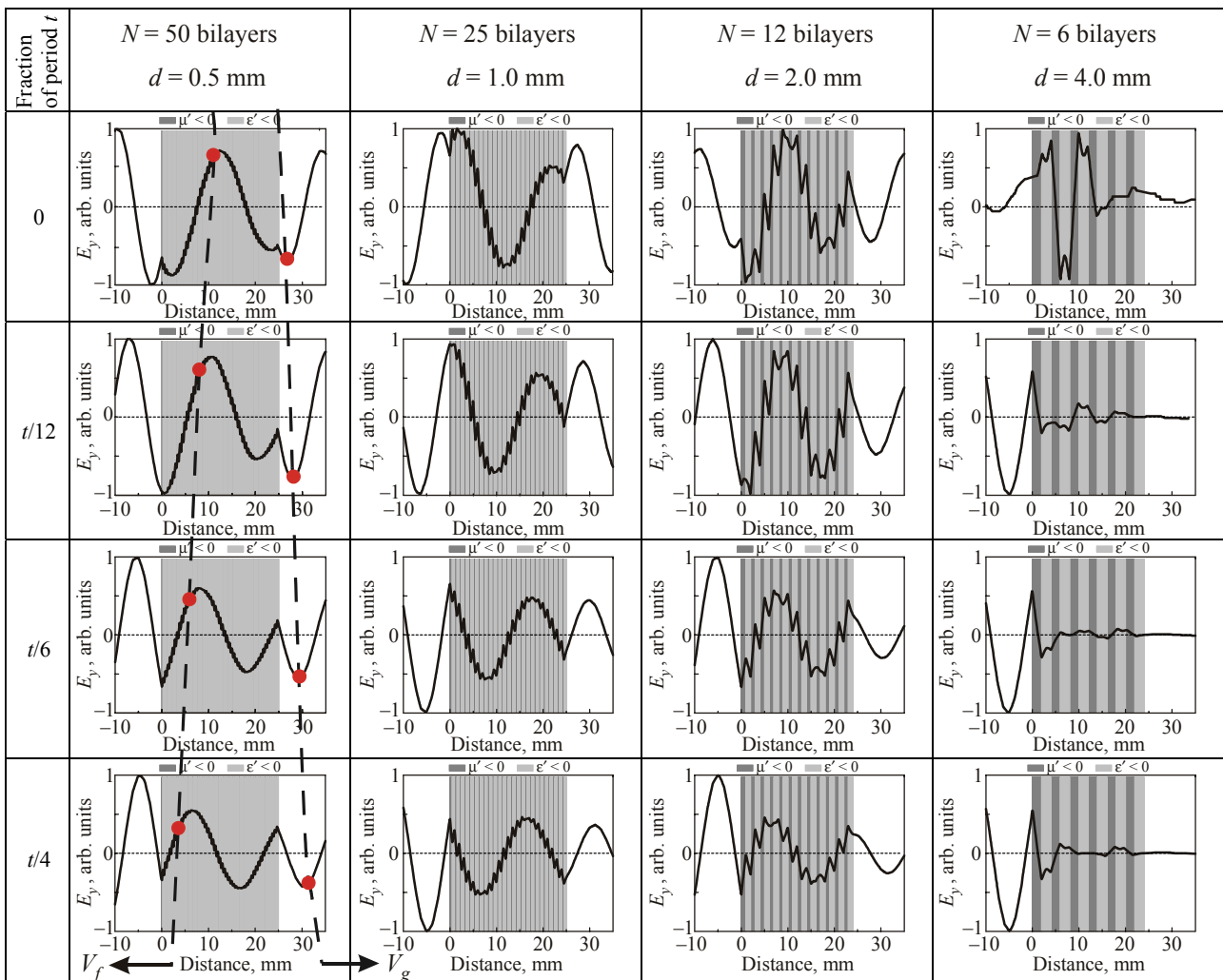


Fig. 21.  $E_y$  distribution along  $Z$  axis for metamaterial with various dispersity (with different thickness of elementary cell  $d$  at permanent metamaterial length) at  $f = 26$  GHz for various time moments.

sented in Fig. 21 for various time moments. Properties of the composite change together with the thickness of elementary cell (or corresponding number  $N$  of bilayers). As can be seen from Fig. 21 a backward-wave, which changes the sign of its phase velocity  $V_f$  after entering the composite medium, appears only for  $N = 50$  bilayers (the average layer thickness  $d = 0.5$  mm),  $N = 25$  and 12 bilayers ( $d = 1.0$  mm and  $d = 2.0$  mm). For  $N < 12$  the attenuation becomes significant so for  $N = 6$  we cannot even talk about the wave as an alternating sequence of maxima.

Therefore we see that besides the condition  $\lambda \gg d$ , the concept of composite as a “continuous” left-handed medium, after entering which the electromagnetic wave changes sign of its phase velocity  $V_f$ , is valid only for sufficiently fine-dispersed composite structure. As about the group velocity ( $V_g$ ) its direction remains unchanged.

Regarding the second case where metamaterial is formed by real media, the physical behavior remains the same one. Namely, the backward wave reveals clearly at  $N > 6$ . The losses, which present in ferrite and wire medium, result in the attenuation of such backward wave propagating through the metamaterial.

### 3.2. Transmission of electromagnetic waves in a fine-stratified ferrite/semiconductor structure

It is known that in periodic ferrite-semiconductor multilayer composite the left-handed behavior is possible [10–12,33–35].

The theoretical and experimental study of the peculiarities of transmission spectra of the TE electromagnetic wave normally incident from the uniform medium onto the fine-stratified structure are presented here. The permeability and permittivity of fine stratified structure are obtained in the long-wave limit. The structure is fabricated by periodic alternating ferrite and semiconductor layers.

The periodic structure where ferrite layers of thickness  $d_1$  and semiconductor layers of thickness  $d_2$  alternate is shown in Fig. 22. An external magnetic field  $\mathbf{H}_0$  is parallel to the  $y$  axis. The thickness of the structure is  $L$  ( $L = Nd$ , where  $N$  is the number of periods,  $d = d_1 + d_2$  is the period of the structure). The structure is placed between homogeneous media with the dielectric permittivities  $\epsilon_a$  and  $\epsilon_b$ ;  $\epsilon_f$  is the permittivity of ferrite layer;  $\epsilon_{yy} = \epsilon_0 \{1 - \omega_p^2 / [\omega(\omega + i\nu)]\}$  is the permittivity of semiconductor layer,  $\epsilon_0$  is the part of the permittivity at-

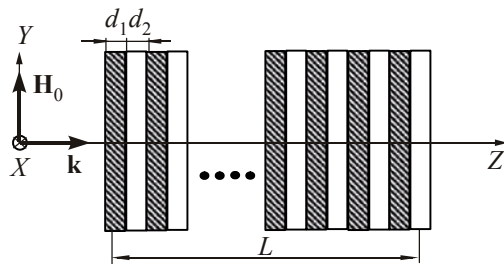


Fig. 22. Scheme of the structure.

tributed to the lattice,  $\omega_p$  is the plasma frequency,  $\nu$  is the collision frequency,  $\mu_f = \mu_{\parallel} + \mu_{\perp}^2 / \mu_{\parallel}$  is the effective permeability of ferrite layer. Its components given in Sec. 2.7 of the given review and [23,24]).

The structure is homogeneous in  $x$  and  $y$  directions, Maxwell equations split into independent equations for two modes with different polarizations. We consider the TE polarization with components  $H_x, H_z, E_y$ . Using the method of the transfer matrix (which relates the fields at the beginning of a wave period and at its end) and applying the Floquet theorem, which takes into account the periodicity of the structure, we obtain the following dispersion relation for the infinite periodic structure:

$$\begin{aligned} \cos \bar{k}d &= \cos k_{z1}d_1 \cos k_{z2}d_2 - \\ &- \frac{1}{2} \left[ \frac{k_{z1}}{k_{z2}} \frac{1}{\mu_F} + \frac{k_{z2}}{k_{z1}} \mu_F - \frac{k_x^2}{k_{z1}k_{z2}\mu_F} \left( \frac{\mu_{\perp}}{\mu_{\parallel}} \right)^2 \right] \times \\ &\times \sin k_{z1}d_1 \sin k_{z2}d_2. \end{aligned} \quad (3.1)$$

Here  $\bar{k}$  is the averaged wave number describing the periodicity of the structure (Bloch wave number). The analysis of expression for effective permeability of ferrite layer  $\mu_f$  following the way used in [23,24,36] and described in the Sec. 2.7 of review reveals 3 characteristic frequencies:  $\omega_1$ ,  $\omega_2$ , and  $\omega_3$ .

Equation (3.1) is studied in the case of a fine-layered medium; i.e.,  $k_{z1}d_1, k_{z2}d_2 \ll 1$ . As the result it is possible to expand the trigonometrical functions into the series. If  $k_x = 0$ , the dispersion relation takes the form [12] (*the case of normal incidence of plane electromagnetic wave* ( $k_x = 0$ )).

$$k_z^2 = \frac{\omega^2}{c^2} \mu^* \epsilon^*, \quad (3.2)$$

where  $\epsilon^* = (d_1\epsilon_f + d_2\epsilon_{yy})/d$ ,  $\mu^* = \mu_{xx}$ . Figure 23 shows frequency dependencies of the effective parameters  $\epsilon^*$  (dashed line) and  $\mu^*$  (solid line), here  $f = \omega/2\pi$ .

The calculations were executed for:  $\epsilon_f = 11.1$ ,  $\omega_M = 84.49$  GHz,  $d_2 = 0.5$  mm,  $\epsilon_0 = 17.8$ ,  $\omega_p = 100$  GHz,  $g = 2$ ,  $d_1 = 0.5$  mm,  $H_0 = 5$  kOe. The collision frequency in the semiconductor layers and magnetic damping in the ferrite were ignored. In Fig. 23, in the frequency range  $\omega_1 < \omega < \omega_4$

$$\omega_4 = \sqrt{\left( \omega_H + \omega_M \frac{d_1}{d} \right) (\omega_H + \omega_M)},$$

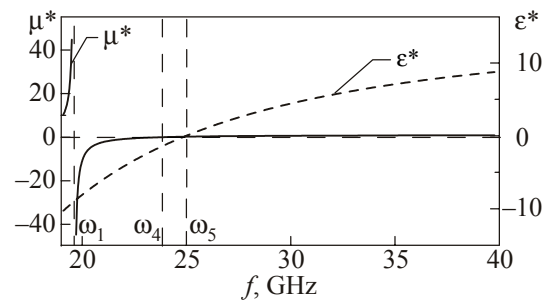


Fig. 23. The frequency dependencies of the effective parameters [24].

the effective permeability  $\mu^*$  is negative. For  $\omega < \omega_5$ ,

$$\omega_5 = \frac{\omega_p \sqrt{\epsilon_0 d_2}}{\sqrt{\epsilon_0 d_2 + \epsilon_f d_1}}, \quad \epsilon^* < 0.$$

Hence, for  $\omega_4 < \omega_5$ , in the frequency range  $\omega_1 < \omega < \omega_4$  one have the composite with the left-handed behavior.

### 3.2.1. Transmission spectra of the structure

The expressions for reflection and transmission coefficients [24] are

$$R = \frac{k_z \mu^* \cos k_z L (k_{za} - k_{zb}) + i \sin k_z L (k_z^2 - k_{za} k_{zb} \mu^{*2})}{k_z \mu^* \cos k_z L (k_{za} + k_{zb}) - i \sin k_z L (k_z^2 + k_{za} k_{zb} \mu^{*2})},$$

$$T = \frac{2e^{-ik_{zb}L} k_z k_{za} \mu^*}{k_z \mu^* \cos k_z L (k_{za} + k_{zb}) - i \sin k_z L (k_z^2 + k_{za} k_{zb} \mu^{*2})}, \quad (3.3)$$

Let us determine the conditions under which the reflectance is equal to zero. From the formulas (3.3), it follows that if the condition  $\epsilon_a = \epsilon^*/\mu^*$  takes place, we obtain the additional one point of full transmittance, let us call this point as *impedance equality peak (IEP)*.

Figure 24 shows the transmission  $|T|^2$  versus frequency at  $H_0 = 5$  kOe ( $\epsilon_f = 11.1$ ,  $\omega_M = 84.49$  GHz,  $\epsilon_0 = 17.8$ ,  $\omega_p = 100$  GHz,  $g = 2$ ,  $d_1 = 0.5$  mm,  $d_2 = 0.5$  mm). The calculations were performed for 3 periods ( $N = 3$ ),  $\epsilon_a = \epsilon_b = 1$  (i.e., the uniform media are vacuum). The solid line is given for  $\omega_r = 0$ ,  $\nu = 0$ ; chain curve corresponds to  $\omega_r = 0.106$  GHz,  $\nu = 1$  GHz; dashed one is for  $\omega_r = 0.106$  GHz,  $\nu = 10$  GHz. It can be seen that when the dissipation is taken into account, the transmission decreases with increasing collision frequency in semiconductor layer. The frequency dependences of the effective  $\epsilon^*$  and  $\mu^*$  are presented in Fig. 23. The frequency range  $24.9$  GHz  $< f < 40$  GHz corresponds to the right-handed material (RHM). First maximum (peak number 1 in Fig. 24) of the transmission at frequency  $f \approx 25.2$  GHz (solid curve) is connected with an implementation of the condition for the IEP in the RHM. The rest of the maximums (2 and 3) are explained by the Wolf-Bragg resonances (WBR in

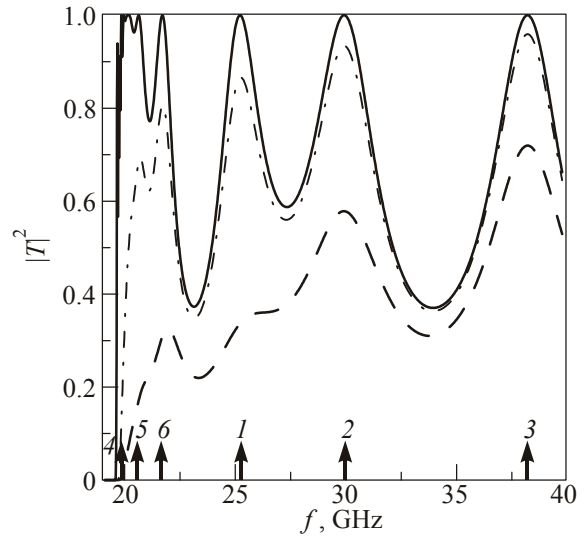


Fig. 24.  $|T|^2$  as a function of the frequency  $f$  for various collision frequencies [24].

RHM). At the range  $19.6$  GHz  $< f < 23.8$  GHz, we obtain the left-handed material (LHM). It can be seen that in this diapason we have some additional peaks of transmission. The maximum 4 of the transmission (solid curve) is connected with an implementation of the condition  $\epsilon^*/\mu^* = 1$  for IEP in LHM. The peaks 5 and 6 are explained by the Wolf-Bragg resonances in the LHM (WBR in LHM).

### 3.2.2. Experiment

The transmission coefficient was measured in the 22–40 GHz frequency range. The external static magnetic field  $\mathbf{H}_0$  was changed in the range of 0–11 kOe and applied normally to alternating magnetic field (Fig. 22).

In Fig. 25 the results of experimental investigations of the transmission spectra of composite structure and its components are presented. Curves 3 (green and blue color online) correspond to the spectra of composites, curves 1 (grey) describe the spectra of InSb plate (thickness of 0.5 mm) and black ones (curves 2) are for the spectra of ferrite plate (thickness of 0.5 mm). Note the expected FMR

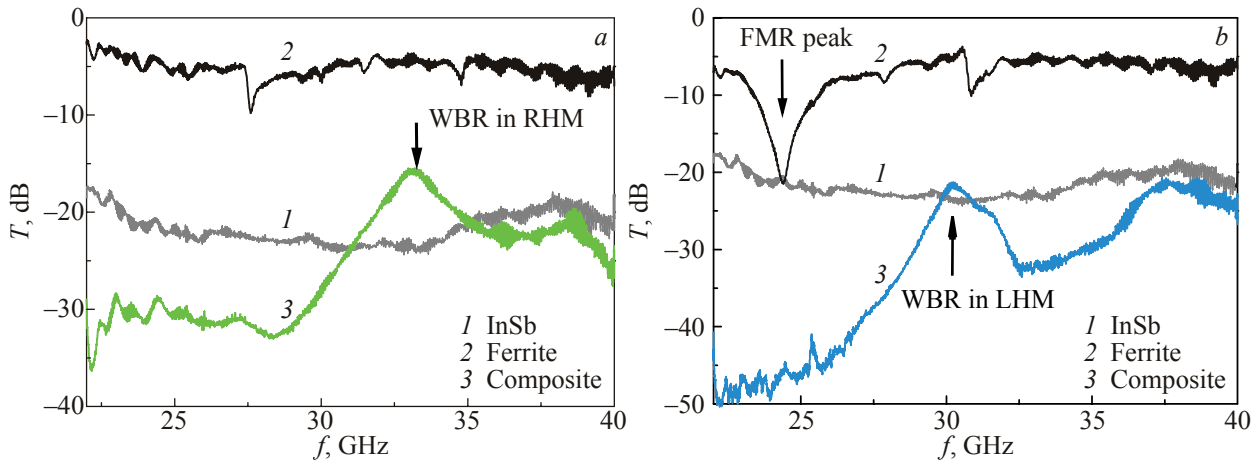


Fig. 25. Transmission spectra of various structures:  $H_0 = 0$  Oe, WBR in RHM (a);  $H_0 = 6570$  Oe, WBR in LHM (b).

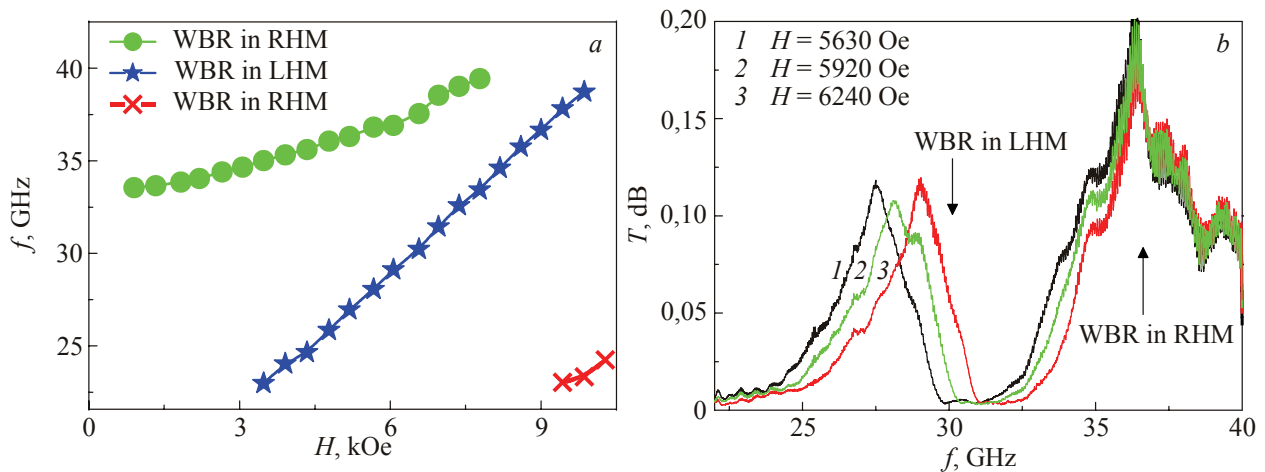


Fig. 26. Experimental dependence of resonance peaks position on magnetic field. One can watch as well an appearance of low-frequency mode (satellite one) of WBR in RHM at  $H > 9$  kOe (crosses) (a); transmission spectra of ferrite/semiconductor composite at various fields (b).

peak appears in spectra for ferrite specimen in Fig. 25,b. One can see that for magnetic field  $H_0 = 0$  Oe the some transmission peak appears in the spectrum of the composite structure (Fig. 25,a). Accordingly to the calculations above the origin of this peak should be associated with WBR in RHM. For large magnetic fields (for example  $H_0 = 6570$  Oe) the transparency resonance peak, which should be associated with WBR in LHM, appears (Fig. 25,b).

The detuning of WBR in RHM and WBR in LHM with the magnetic field is shown in Fig. 26. It should be noted that the steepness of the curve of detuning WBR in RHM ( $\partial f_{WBRinRHM} / \partial H = 1.02$  GHz/kOe) by the magnetic field is less than the corresponding steepness of detuning WBR in LHM ( $\partial f_{WBRinLHM} / \partial H = 2.48$  GHz/kOe). Such behavior can be explained by the strong dependence of WBR in LHM position on the effective negative permeability region associated with FMR behavior.

According to Fig. 26,b the WBR in LHM peak shifts more noticeable that WBR in RHM. Let us note that ex-

perimental peak marked as WBR in LHM coincides with peak 6 in Fig. 24 and peak marked as WBR in RHM coincides with peak 1 in Fig. 24 with accuracy of the experiment. Thus we can conclude that the theoretical model developed in [24] rather well describes the main electromagnetic processes in the structure under study. However, it is necessary to note that, so we carried out experiments at room temperature, the IEP peaks didn't manifest themselves in the spectra detected. The obvious reason of this is a rather high damping in the layers.

### 3.3. Left-handed properties of semiconductor/ferrite composite. Transparency improving

A composite structure formed by semiconductor and ferrite is studied experimentally in the millimetre waveband at room temperature. It was shown before theoretically that such composite structure can manifest LH properties [32,37].

The one-dimensional structure was used in experiment (Fig. 27) is presented below. The composite structure con-

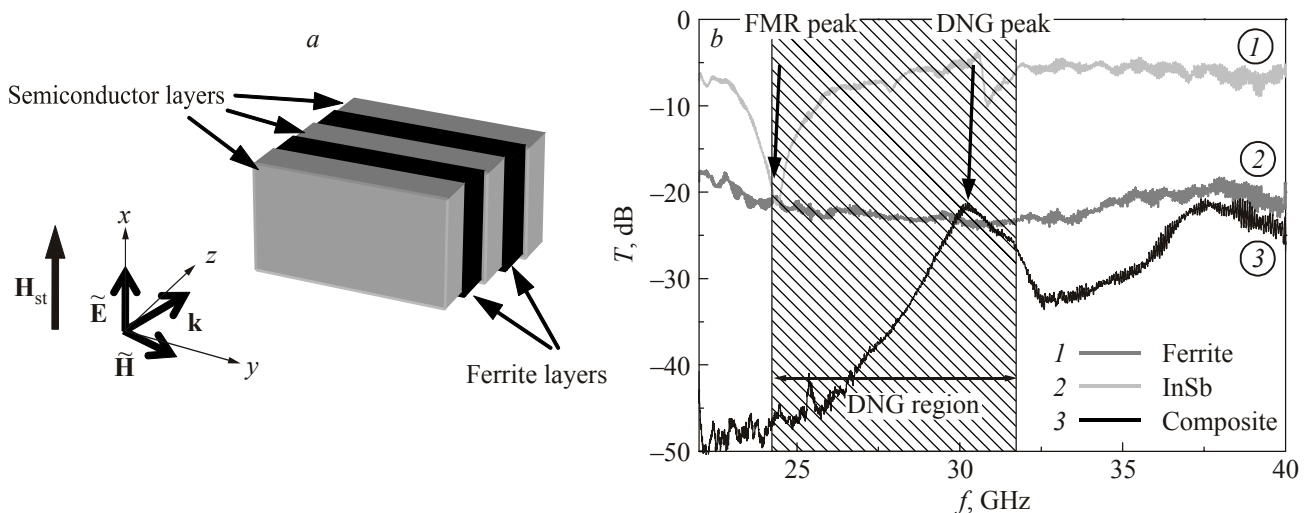


Fig. 27. The composite structure under study (a) and the transmission spectra of various structures at  $H = 6570$  Oe (b).

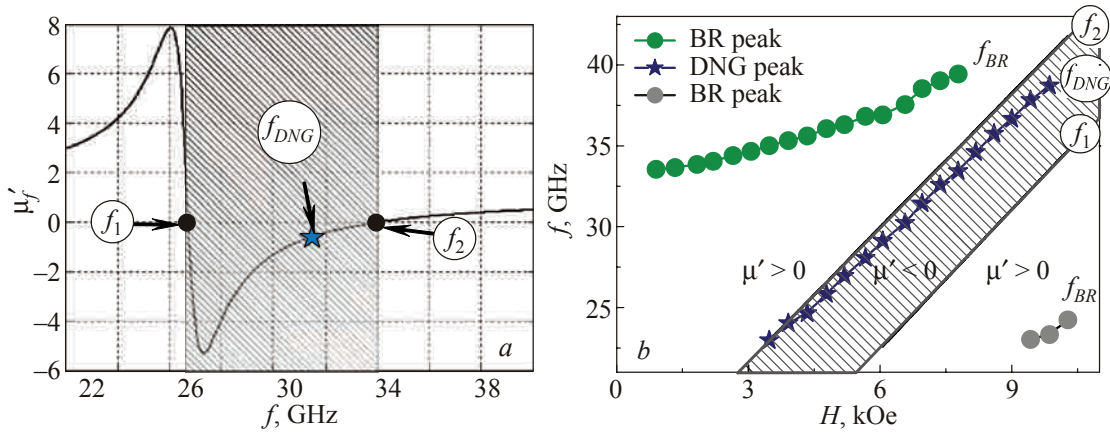


Fig. 28. Calculated ferrite permeability real part at  $H = 6570$  Oe (a); the character peaks position versus magnetic field (b).

sists of alternating ferrite (brand 1SCH4) and InSb semiconductor layers with ( $\lambda \gg d$ ): 3 semiconductor layers and 2 ferrite layers (Fig. 27,a). (see details in [32]). The composite structure is embedded into a hollow rectangular metal waveguide. Electromagnetic wave propagates along  $z$  axis its electric vector is directed along  $x$  axis and its magnetic vector along  $Y$  axis. The external static magnetic field  $\mathbf{H}_{st}$  applied in parallel with alternating electric field (Fig. 27,a). The transmission coefficient was measured in the 22–40 GHz frequency range.

In the frequency range, where effective permittivity and permeability of the composite structure are both negative:  $\epsilon'_{eff} < 0$  and  $\mu'_{eff} < 0$ , the transmission double negative (DNG) peak can be registered. The effective permittivity is negative in the whole investigated frequency range due to negativity of semiconductor layer permittivity [39]. The effective permeability of composite structure is negative near the ferrite FMR frequency because the ferrite layer permeability is negative in high frequency vicinity of FMR [9].

In Fig. 28 the experimental transmission spectra of composite structure for  $H = 6570$  Oe are presented. The transparency peak appears associated with LHM properties of the structure. To clarify the origin of this peak we calculated the dependence on frequency of the real part of ferrite permeability according to [9,45]. The typical dependence  $\mu'_f(f)$  for  $H = 6570$  Oe is shown (Fig. 28,a), where  $f_1$  and  $f_2$  are the left and right frequency borders of the area, where  $\mu' < 0$ ;  $f_{BR}$  is frequency position of Bragg resonance transmission peaks. As shown on Fig. 28,b this peak is located in the DNG region  $\epsilon'_{eff} < 0$  and  $\mu'_{eff} < 0$  (DNG peak). The magnetic field tuning of resonance peaks position is presented on Fig. 28,b.

### 3.4. The negative refraction in ferrite/semiconductor composite

One method of verification of left-handed properties of metamaterial is based on T-junction waveguide measurement [40]. Here we provide the corresponding experi-

mental measurements for 2D metamaterial prism build from ferrite and semiconductor bricks alternating in a staggered order. The arrangement guarantees higher degree of composite homogenization and should demonstrate its left-handed properties more clearly.

The two-dimensional structure was used in experiment (Fig. 29). The composite prism type 45–90–45 degree, used in the experiment (Fig. 29) consists of ferrite and semiconductor ( $n$ -InSb) bricks, alternating in a staggered order [41]. The triangle prism is formed by 72 rectangular-bar elements. An electromagnetic wave propagates along the  $z$  axis with an electric field along the  $x$  axis and magnetic field along the  $y$  axis. The external static magnetic field  $\mathbf{H}_0$  applied normally to alternating magnetic field.

We investigated the transmission properties of the prism just in the frequency band, where effective negative composite permittivity  $\epsilon'_{eff}$  and composite negative permeability  $\mu'_{eff}$  both were negative. The transmission DNG peak can be registered in this band [9]. The transition to the left-handed state drastically changes the refraction in the prism making the electromagnetic wave to change its way in T-junction.

The transmission through T-junction was calibrated to zero level at  $H = 0$  Oe. Experimental results on measuring the transmission spectrum of the composite prism at magnetic field 7240 Oe are given in Fig. 30,a.

It is seen that at the DNG zone of the prism near the frequency of  $f_{DNG} = 34.6$  GHz the transparency peak

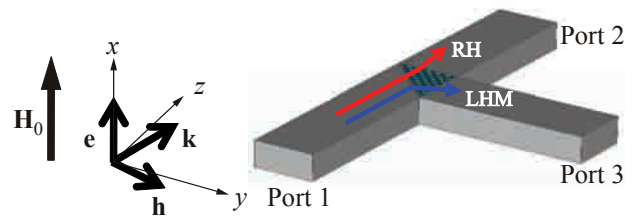


Fig. 29. The T-junction waveguide with metamaterial prism: scheme.

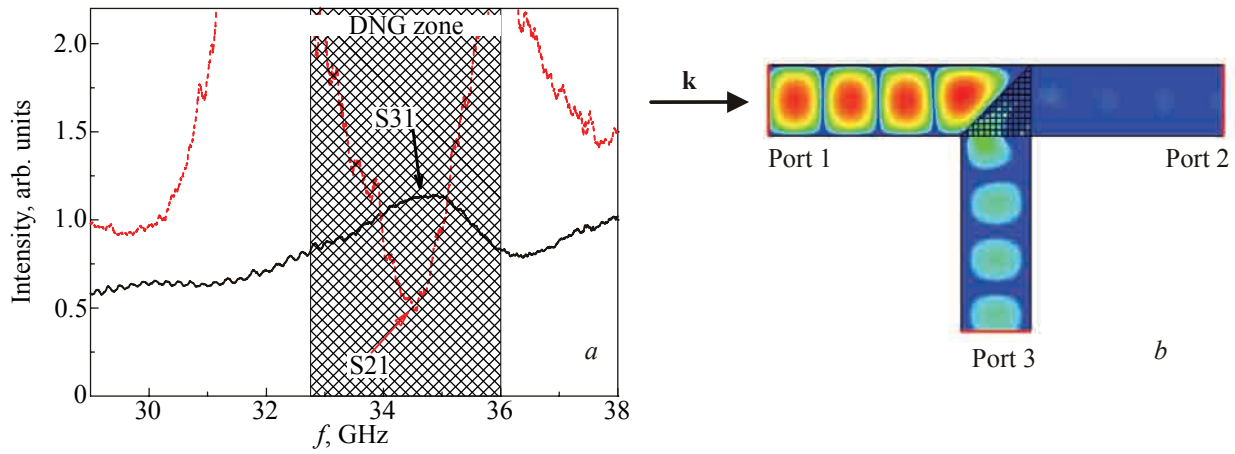


Fig. 30. Experimental results for transmission spectrum of the composite prism on magnetic field 7240 Oe (a); the spatial distribution of *e*-component of the extra high-frequency field for T-junction ( $H = 7240$  Oe,  $f = 36.2$  GHz) (b).

(DNG peak) appears at the port 3 (S31) and disappears at the port 2 (S21) (Fig. 30,a). This transparency peak should be associated with the negative refraction in a prism. To verify this fact we take into account that a backward wave in metamaterial takes place at the frequency of maximum transparency ( $f_{DNG}$ ). We have calculated by FDTD method the spatial distribution of electromagnetic field in the composite prism at the frequency of  $f_{DNG} = 36.2$  GHz and various values of magnetic field. The field pattern at  $H = 7240$  Oe is presented in Fig. 30,b. The electromagnetic wave turns to the port 3 (S31). At the same time the electromagnetic wave damps out in the direction of the port 2 (S21). Thus the scenario testifies that the prism demonstrates left-handed behavior, namely the negative refraction takes place.

### 3.5. Left-handed properties of ferrite/metal based composites (ferrite/wire medium, ferrite/thin metal plates)

The LHM metamaterial, composed by ferrite layers (negative permeability) and (negative permittivity) metal deposited wires (Wire medium WM) or Cu-, Ni-plate structure are investigated here. A WM is formed by wire

grids. The frequency dependence of the WM permittivity  $\epsilon_{WM} = \phi(f)$  is described by known Drude formula for free electron gas,  $\epsilon_{WM}(f) = \epsilon_{\text{host}} - f_{pWM}^2/f^2$ , where  $f$  is the frequency and  $\epsilon_{\text{host}}$  is the permittivity of the host media (media, where WM is located). The  $f_{pWM}$  is a parameter depending on wires configuration — an “effective plasma frequency”,  $f_{pWM}^2 = c^2/[a^2 \ln(a/r)]$  where  $a$ ,  $r$  are the distance between wires and their diameters,  $c$  is the light velocity. The varying of the parameter  $f_{pWM}$  makes it possible to narrow down frequency band of LHM existence to millimetre wavelength band. It was found the frequency range, where the LHM transmission coefficient is quite high. This frequency band, called as DNG region [42], is connected with appearance of LHM properties and lies near the FMR peak for the ferrite.

#### 3.5.1. Ferrite/WM structure

The first investigated structure consists of three flat parallel ferrite plates alternating with four polystyrene plates with deposited flat copper wires (Fig. 31) see details in [43]. The static magnetic field ( $H_{st} = 0-7$  kOe) vector was directed perpendicularly to alternating magnetic field vector  $\tilde{H}$  (see Fig. 31). Note that the optical width value of

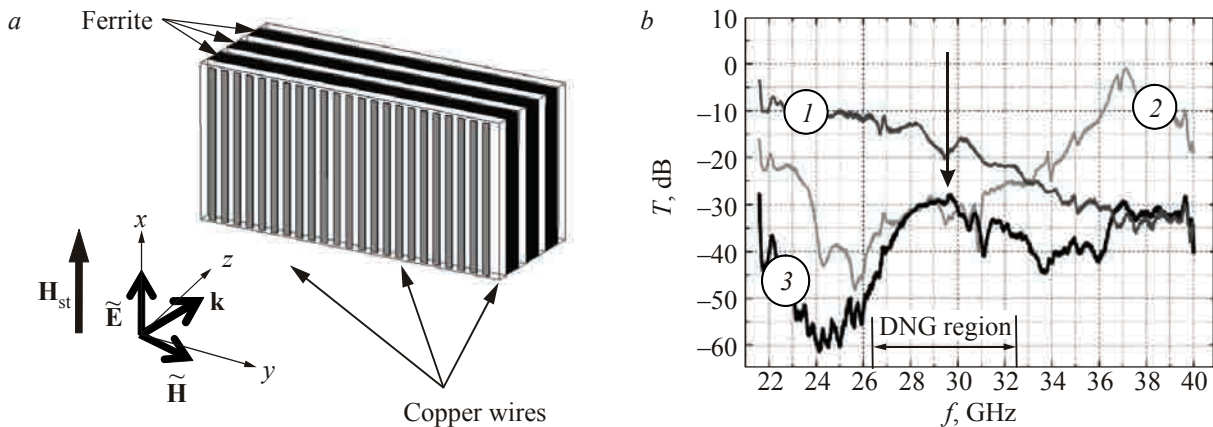


Fig. 31. Ferrite/wire medium structure (a). Experimental transmission coefficient for ferrite/wire medium structure and its components.  $H_{st} = 6.84$  kOe. WM (1), ferrite layer medium (2), ferrite/wire medium structure (3) (b).

each element of LHM is approximately 5 times less than the wavelength. So we can use terms “the effective/averaged permittivity/permeability of the medium” to describe the given structure with effective constitutive parameters.

Experimental results are presented in Fig. 31,*b*. One can see there spectra: for WM (curve 1), for ferrite-layer medium (curve 2) and for ferrite/wire-medium structure (curve 3). Experimental results show the presence of the transmission peak in the band of 26.5–32.0 GHz having maximum height of –30 dB (arrow in Fig. 31,*b*). The height of this transmission peak is almost 20 dB higher than additive transmission coefficients formed by formal summing of coefficients for wire-medium (1) and ferrite layers (2) at the given frequency range. This peak is an analog of the peak corresponded to DNG region and studied for example in [42]. Note that for 26.5–32.5 GHz both of effective constitutive parameters are negative, that means the appearance of LHM. Also the tuning of position of DNG region by magnetic field was observed. This is connected with change of FMR position with external magnetic field  $\mathbf{H}_{st}$ . Note that ferrite demonstrates a negative permeability for some definite range of magnetic field. These fields are in the high-frequency vicinity of the FMR peak [45]. The effective permittivity remains negative, because the plasma frequency [44] for given WM is about 300 GHz.

### 3.5.2. Ferrite/thin-metal-layer structure

In order to define the LHM conditions for the medium, where the negative permittivity is formed by material with spatially homogeneous constitutive parameters, a thin metal plane was used instead of wires. This experimental realization of the LHM composite consists of the same ferrite layers, with thin copper (or nickel) layers deposited on mica substrate between them (see details in [43]).

The results are shown in Fig. 32. As in Fig. 31,*b* the spectra of thin-metal-layer structure (curve 1), of ferrite-layer medium (curve 2) and of ferrite/thin-metal layer structure (curve 3) are presented here. The transmission

peaks (DNG regions) are also present here. In the case of nickel layers it is in the frequency band 26.5–33.0 GHz.

As follows from Fig. 32,*b* for the case of copper layers the left-handed behavior of the composite is more well-defined. Namely, the DNG region, which appears in the band 27.0–34.0 GHz with maximum height –8 dB (arrow in Fig. 32,*b*) is almost 30 dB bigger than the additive transmission coefficient. Thus from Fig. 32,*b* it follows that for frequency band 33.0–33.5 GHz the maximum of transmission coefficient of composite structure exceeds the sum of transmission coefficients of composing materials. Probably this phenomenon is caused by the optimal matching between the structure elements.

### 3.6. Left-handed behavior of strontium-doped lanthanum manganite

Left-handed behavior of strontium-doped lanthanum manganite was revealed in the millimeter waveband. The bulk specimen of  $\text{La}_{1-x}\text{Sr}_x\text{MnO}_3$ , was used as a boundary medium for 1D PC. In the absence of magnetic field known Tamm peak appears in the forbidden zone of PC indicating that manganite is a single negative medium (negative permittivity). In the presence of external magnetic field somewhat above frequency of ferromagnetic resonance the additional (field sensitive) transparency peak appears in PC forbidden zone, indicating that manganite becomes double negative medium (negative permittivity and permeability). Model theoretical calculations corroborate the experimental findings.

The compounds of the  $\text{La}_{1-x}\text{M}_x\text{MnO}_3$  system, where M is a divalent element, are crystallized in perovskite structure [30,46]. Specific feature of such materials is a phase transition from ferromagnetic metallic to paramagnetic dielectric state [29]. The temperature of the phase transition (Curie temperature,  $T_C$ ) can be changed by changing concentration of doping element [29]. In films studied in [28], calcium was chosen as a doping element. Note that  $T_C$  for whole range of replacements [29] of  $\text{La}_{1-x}\text{Ca}_x\text{MnO}_3$  system lies below the room temperature.

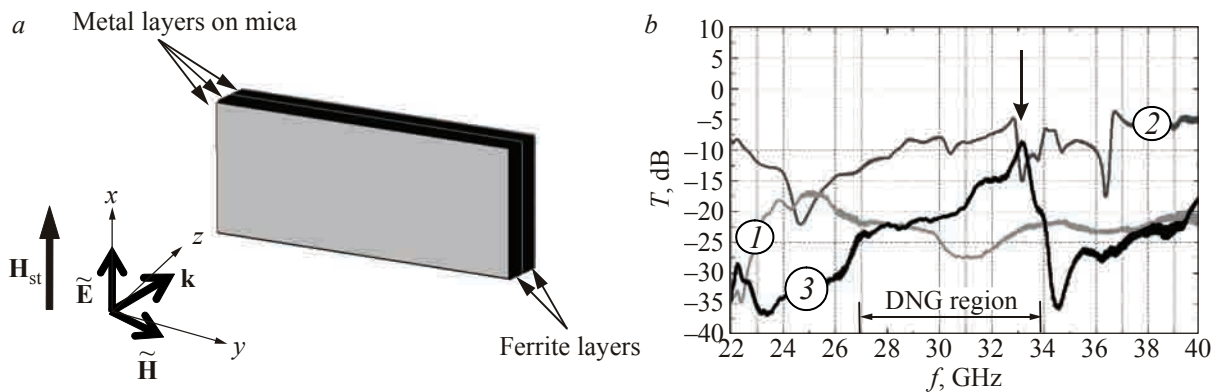


Fig. 32. Ferrite/thin-metal layer structure (a); the experimental transmission coefficient for ferrite/thin-metal layer structure.  $H_{st} = 7.0$  kOe. Copper thin metal layer structure (1), ferrite medium (2), composite structure (3) (b).

In strontium-doped lanthanum manganite  $\text{La}_{1-x}\text{Sr}_x\text{MnO}_3$ , employed in this study,  $T_C$  is above the room temperature ( $T_C = 350$  K) for concentrations within the range  $x \approx 0.2-0.5$  [29,47]. This fact is evidently of great importance for future potential applications.

This study gives strong experimental evidence of existence LHM in strontium-doped lanthanum manganite  $\text{La}_{1-x}\text{Sr}_x\text{MnO}_3$  ( $x = 0.225$ ) in external applied magnetic field, which control the appearance of left handed behavior.

A one-dimensional photonic crystal [9,29] was assembled of 6–8 double cells (bilayers). Each cell consisted of teflon and quartz layers (Fig. 33). The PC parameters have been chosen in order to obtain the forbidden zone at 22–40 GHz [31]. It is known [7,29,49] that if a PC interfaces with a conductor, a Tamm peak appears in the PC forbidden zone. Tamm-peak width, frequency and amplitude depend on effective constitutive parameters of the boundary medium. In our experiments the  $\text{La}_{0.775}\text{Sr}_{0.225}\text{MnO}_3$  specimen (Fig. 33) was used as a boundary medium. The specimen was synthesized by conventional solid-state technology [29,30]. The system, PC with the medium, was embedded into a waveguide and located between poles of an electromagnet. Electrodynamic spectra were registered by the Network Analyzer at magnetic fields up to 7500 Oe. The vector of a permanent magnetic field is parallel to PC layers and is directed normally to the magnetic component of alternating field.

A typical forbidden zone detected experimentally in PC transmission spectrum in the absence of the boundary medium is shown in Fig. 34,a. In the presence of manganite-perovskite specimen at the PC boundary, a Tamm peak (peak 1) appeared in the forbidden zone (Fig. 34,b). Note, that its quality factor  $Q$  is about  $10^2$  and depends on the number of PC bilayers.

When a static magnetic field is applied, a second peak (the DNG peak, peak 2) appears in the PC forbidden zone (Fig. 34,c). The quality factor of the second peak is lower, as compared with Tamm-peak  $Q$ -factor.

The temperature of the system does not affect noticeably the peak 1, at the same time it changes essentially the peak 2. In particular, the intensity of the peak 2 decreases as the temperature increases. The peak 2 disappears com-

pletely at temperature  $T_C \geq 350$  K. This fact is natural, because as it was shown [18,29,30,50], up to  $T = 350$  K the  $\text{La}_{0.775}\text{Sr}_{0.225}\text{MnO}_3$  specimen (further — the specimen) is a metallic ferromagnetic (having negative permeability in the vicinity of the ferromagnetic resonance) and above 350 K is the paramagnetic.

We elucidate the observed phenomena assuming LHM behavior of the manganite boundary medium high-conductive medium at the boundary of 1D PC (Fig. 33), gives rise to surface oscillations of electromagnetic field, known as Tamm surface state [7,29]. Tamm state manifests itself as a narrow peak (Tamm peak) in forbidden zone. The experimental position of the Tamm peak (peak 1) (Fig. 34,b) in the PC forbidden zone confirms the metal-type conductivity (negative permittivity) of the manganite specimen in this temperature range.

In external static magnetic field the specimen can be in FMR conditions. As it is known [28], in high-frequency side of the FMR peak, the real part of the permeability is negative and the imaginary part is rather small (negative permeability zone, NP zone). For our specimen with metal conductivity real parts of permittivity and permeability will be negative in NP zone and the specimen will behave as a left-handed medium. As the magnetic field increases the FMR peak and NP zone move toward higher frequencies. When the NP zone reaches the forbidden zone of PC, the region of high transparency known as double negative zone [42] (DNG zone) appears. In this frequency region a backward wave propagates through the LHM, and consequently the transmission of energy through the whole structure essentially increases. In experiment we see a DNG peak (peak 2) in this frequency region (see Fig. 34,c). The frequency of DNG peak strongly depends on the magnetic field.

To confirm our conclusions based on experimental data, we calculated the transmission spectra for PC, bounded with a model structure with negative permittivity (does not depend on the external magnetic field) and negative permeability (depends on the external magnetic field by known FMR law) (Fig. 34, right). For calculations we used the known matrix method, described in details in the solution of similar problems in [7,29]. Parameters of the calculated PC corresponded to experiment. The permeability and the permittivity of the specimen estimated on the base of FMR experimental data and by the known technique described in [29,48].

According to our calculations, the forbidden zone for the PC in the absence of boundary medium lies in the frequency band 22–40 GHz (Fig. 34,a). When the ferromagnetic conductive boundary medium (at  $H = 0$ ) is attached to PC, then the Tamm peak appears (Fig. 34,b). Due to the boundary medium influence PC pass zones become less pronounced as compared with Tamm peak [49]. The DNG peak (depending on magnetic field) arises in the spectrum when  $H > 0$  and moves towards high-frequency side as the

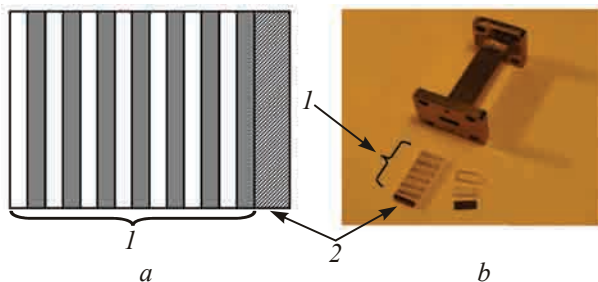


Fig. 33. The structure under study: scheme (a); overview (b): photonic crystal (PC) (1),  $\text{La}_{0.775}\text{Sr}_{0.225}\text{MnO}_3$  specimen (2).

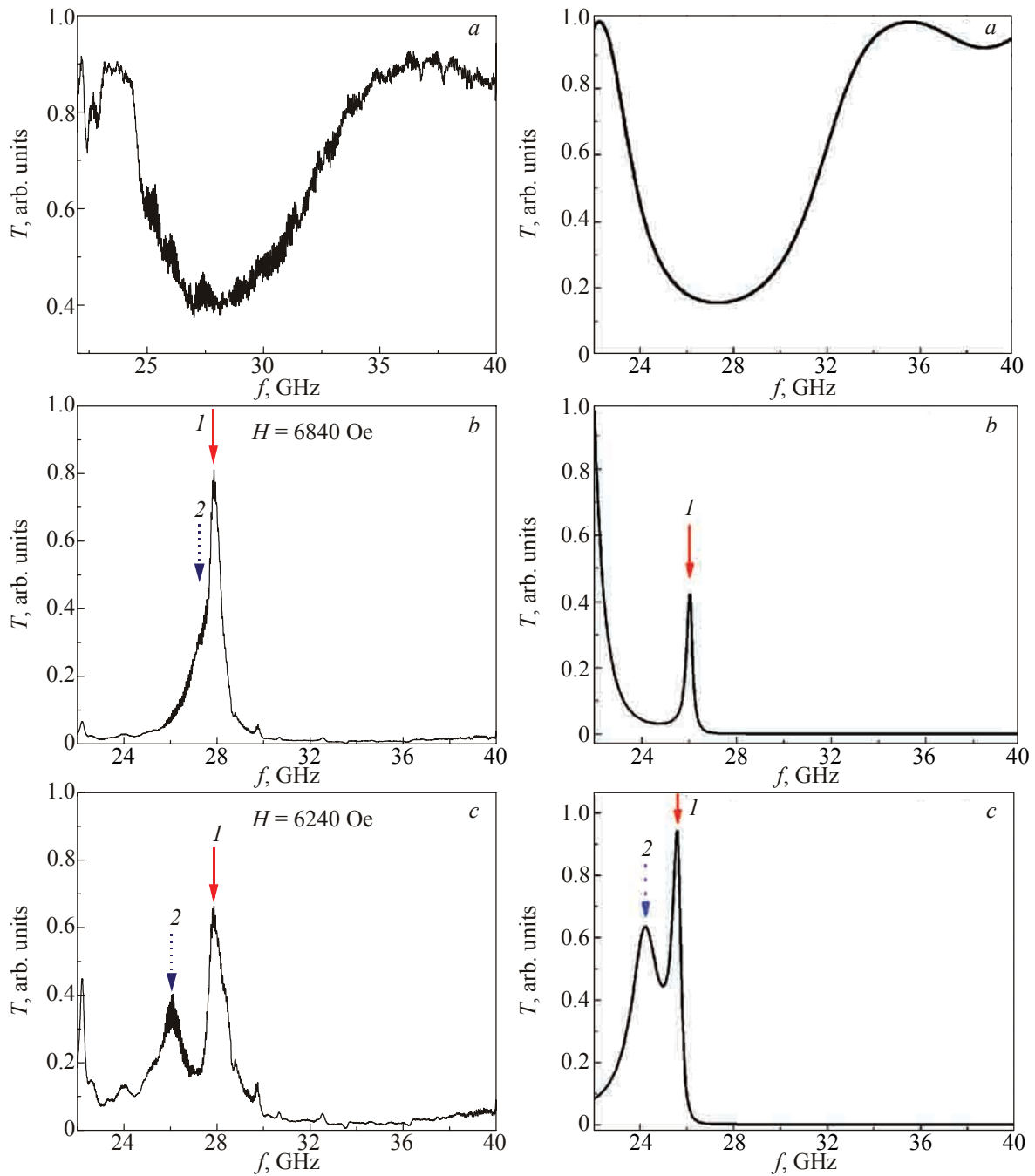


Fig. 34. Experimental (left) and simulated (right) transmission spectra: Forbidden zone for PC without a boundary medium (a); zone spectrum for PC bounded by  $\text{La}_{0.775}\text{Sr}_{0.225}\text{MnO}_3$  specimen (at  $H = 0$ . Red solid arrow — the Tamm peak 1) (b); zone spectrum for PC bounded by ferromagnet conductive medium,  $H > 0$ . Blue dashed arrow — peak 2 (DNG peak) (c).

magnetic field increases. When  $H$  exceeds 5 kOe the DNG peak enters the PC forbidden zone (Fig. 34,c). The calculations describe well the physical processes, observed in our experiments with the specimen  $\text{La}_{0.775}\text{Sr}_{0.225}\text{MnO}_3$ .

### 3.7. Dispersion of negative permittivity of strontium-doped lanthanum manganite

We studied experimentally the  $\text{La}_{0.775}\text{Sr}_{0.225}\text{MnO}_3$  manganite in the frequency band 20–40 GHz and deter-

mined the frequency dependence of its permittivity [51]. It turned out that the frequency dependence of the permittivity is well described by Drude formula with only one parameter — the “effective plasma frequency”. It is noteworthy that the determined value is in compliance with that obtained in [28] from measurements in the frequency band of 80–150 GHz.

In order to demonstrate intrinsic features of the LHM refraction, we have carried out the experiment with refraction in the prism made from bulk  $\text{La}_{0.775}\text{Sr}_{0.225}\text{MnO}_3$  and

placed into T-bridge. The transition of the strontium-doped lanthanum manganite to the LHM state has been accompanied with a sharp ray deflection in T-bridge.

The aim of the given chapter is to show the technique of the measuring the permittivity of the left-handed  $\text{La}_{0.775}\text{Sr}_{0.225}\text{MnO}_3$  manganite.

The specimen represented a 1D finely-stratified medium (Fig. 35) formed by thin ( $d_m \ll \lambda$ ) manganite layers alternating with thin ( $d_t \ll \lambda$ ) teflon layers. The structure was embedded into a single-mode waveguide and the technique of experiment described in [30] was applied. The effective permittivity of the structure is described by the known formula

$$\epsilon_{\text{eff}}(f) = \frac{\epsilon_t d_t + \epsilon_m(f) d_m}{d_m + d_t}, \quad (3.4)$$

where  $\epsilon_t$  and  $\epsilon_m$  are permittivities of teflon and manganite, correspondingly.

The teflon thickness  $d_t$  varies during the experiment, while  $d_m$  remains constant. According to (3.4) for the given frequency  $f$ , the effective permittivity  $\epsilon_{\text{eff}}(f)$  varies with  $d_t$ . In the DNG zone we have  $\epsilon_t > 0$  and  $\epsilon_m < 0$ . The “plasma frequency” of such finely-stratified medium is the frequency at which  $\epsilon_{\text{eff}}(f_p) = 0$ . Thus, as it follows from (3.4) the permittivity of manganite for this frequency is:

$$\epsilon_m(f_p) = -\epsilon_t d_t / d_m. \quad (3.5)$$

To obtain the negative permeability an external magnetic field is applied to the structure with some definite  $d_t^{(i)}$ . The appearance of a DNG zone in the transmission spectrum (see Figures above) indicates that left-handed features of the medium have appeared. In DNG zone we have:

- the permeability of the structure is negative,  $\mu'(f) < 0$ : this frequency zone corresponds to the high-frequency wing of the FMR peak [30], where the real part of permeability  $\mu'(f) < 0$ ;

- the effective permittivity for total structure is negative,  $\epsilon_{\text{eff}}(f) < 0$ : this is possible because every manganite element of the structure (Fig. 35) is a conductor.

As the FMR frequency depends linearly [52] on  $H$ , the DNG zone shifts toward higher frequencies when magnetic field  $H$  increases (Fig. 36,a). The intensity of DNG zone falls down and then zone disappears at the “plasma frequency”  $f_p^{(i)}(d_t^{(i)})$  for given structure (the finely-stratified medium), when its effective permittivity changes the sign to positive,

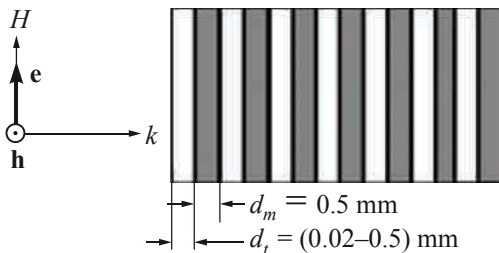


Fig. 35. Configuration of the structure under study.

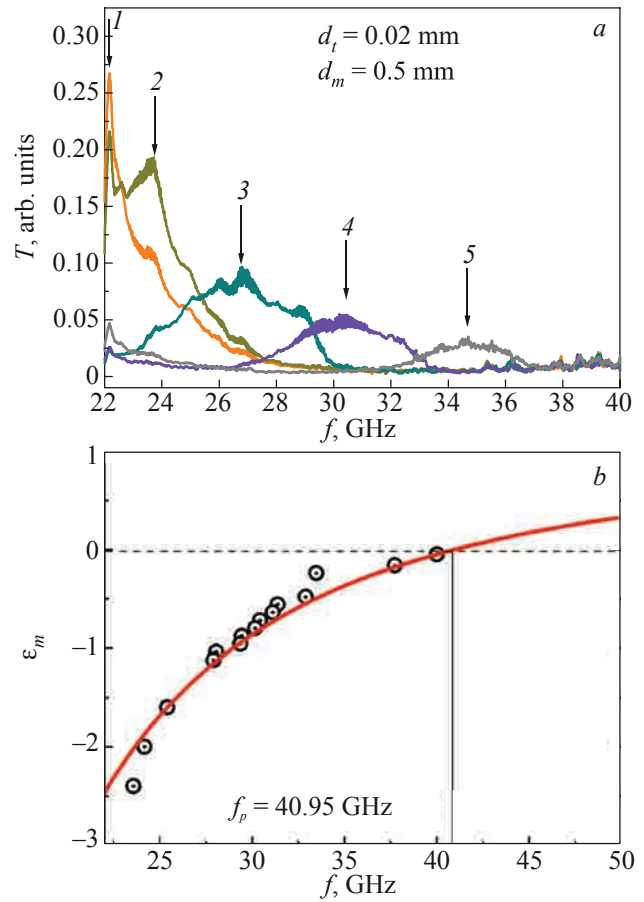


Fig. 36. Typical position of the DNG zone at different magnetic field  $H$ , kOe: 1.1 (1), 1.93 (2), 2.7 (3), 3.42 (4), 4.43 (5) (a); the dispersion curve for sintered lanthanum-strontium manganite  $\text{La}_{0.775}\text{Sr}_{0.225}\text{MnO}_3$  (b).

namely at:  $\epsilon_{\text{eff}}^{(i)}(f) \Big|_{f=f_p^{(i)}} = 0$ . Now from (3.5) we define the magnitude  $\epsilon_m^{(i)}$  of the sintered manganite permittivity at the frequency  $f = f_p^{(i)}$ .

After performing a cycle of measurements with various thickness of teflon layers  $0.02 \text{ mm} \leq d_t^{(i)} \leq 0.5 \text{ mm}$ , we restored the dispersion curve  $\epsilon_m(f) = \varphi(f)$  (Fig. 36,b). The experimental dependence is well described by Drude formula at  $\epsilon_{\text{host}} = 1$ :

$$\epsilon_{WM}(f) = \epsilon_{\text{host}} - (f_p^m)^2 / f^2. \quad (3.6)$$

According to the curve in Fig. 36,b, the “effective plasma frequency” for specimen of sintered lanthanum-strontium manganite  $\text{La}_{0.775}\text{Sr}_{0.225}\text{MnO}_3$ , used in our experiment equals  $f_p^m = (40.95 \pm 1.00) \text{ GHz}$ .

To verify the above results, an experiment, which demonstrates negativity of manganite refractive index has been performed. A conceptual design of this experiment [53] is presented in Appendix (Fig. 40). A prism manufactured from sintered manganite under study is installed into the T-bridge. The external magnetic field  $H$  applied normally to the trigonal face of the prism.

A sharp change in refraction was observed at transition of the medium into left-handed state ( $f = 28 \text{ GHz}$  and mag-

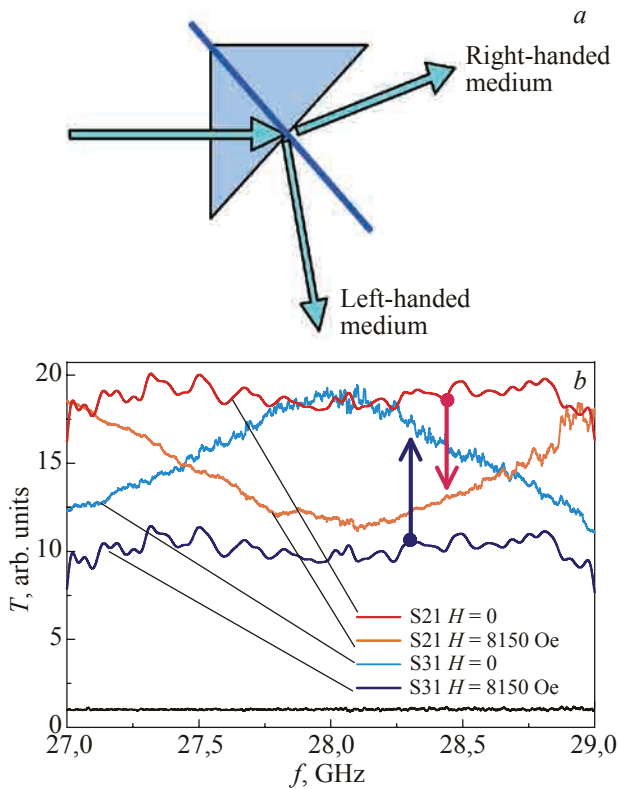


Fig. 37. The ray tracing in the left handed prism [50] (a); the transmission spectra through the “straight” channel (S21) and “perpendicular” channel (S31) for  $H = 0$  and at  $H = 8150$  Oe (b).

netic field  $H = 8150$  Oe). The “beam” propagating initially in the “straight” channel changed its direction to “perpendicular” channel (see Fig. 37,b).

As can be seen in Fig. 37,b at  $H = 8150$  Oe the signal in the “straight” channel (S21) drops while in the “perpendicular” channel (S31) it reaches approximately the value of previous signal in the “straight” channel at  $H = 0$ .

As can be concluded from above the refraction in the specimen is characterized by negative refractive index and consequently both effective permittivity and permeability of such medium become negative at these conditions. The negative permeability of the ferromagnet is known to appear in the vicinity of the FMR, so the frequency of the double negative peak is close to FMR frequency and depends in particular from the saturation magnetization of doped lanthanum manganite. This enabled us to obtain the temperature dependence of the magnetization in the temperature range 270–400 K where phase transition from metallic ferromagnetic to dielectric paramagnetic state takes place. The magnitude of the critical exponent  $\beta$  ( $\beta \approx 0.50$ ) determined in our work [54] agrees with results reported in literature and allows supposing that long-range interactions play an important role in the phase transition from conductive ferromagnetic to nonconductive dielectric paramagnetic state of the manganite in its Curie point.

## APPENDIX. EXPERIMENTAL TECHNIQUE AND STRUCTURES UNDER STUDY

### A.1. Experimental set-ups

The typical scheme of experimental research is presented in Fig. 38 and described in details for example in [4,14]. The Vector Network Analyzer “Agilent N5230A” was used as a generator and detector of microwave radiation. The waveguide transmission line was formed of emitting and detecting hollow metal rectangular waveguides. When experiments were performed in ambient space the horns, which form a plane wavefront were applied Fig. 38,b and a section of single-mode waveguide with embedded specimen under study.

The static magnetic field  $H_0$  was generated with an electromagnet and changed in the range of 0–19 kOe. Its

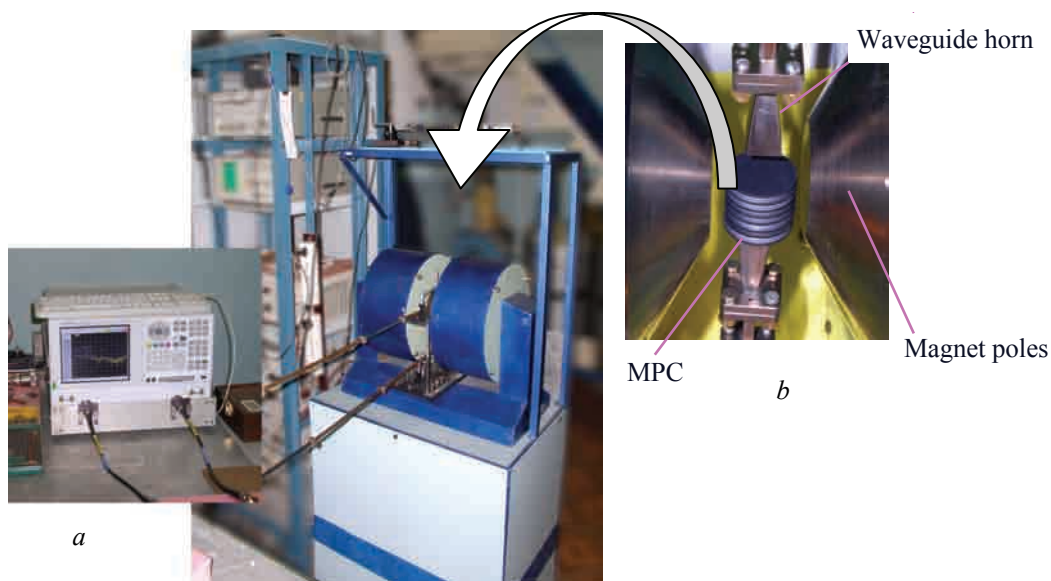


Fig. 38. The photo of the test bench (a) and a typical MPC structure between horns and between poles of magnet (b).

measurement error did not exceed 1%. The nonhomogeneity of the external magnetic field in the volume of structures under study did not exceed 0.5%, which has no appreciable affect on observed effects. The studied structure with magneto-depended elements was placed in a gap of the electromagnet, the static magnetic field  $\mathbf{H}_0$  being perpendicular to the wave vector  $\mathbf{k}$  and to provide the situations either  $\mathbf{H}_0 \perp \mathbf{h}$  or  $\mathbf{H}_0 \parallel \mathbf{h}$ . Note that the possibility of parallel orientation of  $\mathbf{H}_0$  and  $\mathbf{k}$  vectors are provided as well. The wave transmission coefficient was measured mainly in the frequency band of 20–40 GHz.

When the spatial distribution of the electromagnetic field were studied, the digital controlled scanner (Fig. 39) was used. The scanner provides the accuracy no less that 0.1 mm.



Fig. 39. The scanning system for the spatial field distribution in PC detecting.

### A.2. Models of 1D photonic crystals and left handed metamaterials

The typical models of photonic crystals and magnetophotonic crystals manufactured from various elements as well as left handed metamaterials under study are presented below:

#### The 1D photonic crystals for ambient space research

The structures were studied, being embedded into absorbing shielding screen, or without it.



Fig. 40. The axially symmetrical microwave 1D photonic crystals: for ambient space research: ferrite/polystyrene/air-gap MPC (a); teflon/quartz PC; diameter of disks is about  $\approx 5-7 \lambda$  (b).

#### The 1D MPC for waveguide research

The structures were placed into single-mode rectangular (Fig. 41,a,b) or cylindrical Fig. 41,c waveguides.

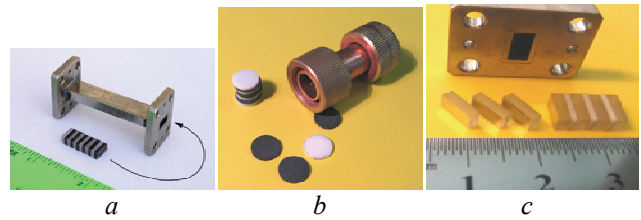


Fig. 41. Ferrite/quartz MPC (a); metal/quartz PC (b); axially symmetrical MPC and PC (ferrite/quartz/teflon) (c). Diameter of disks is about  $\approx \lambda$ .

#### 1D MPC for Tamm state investigation

The elements of PC and MPC together with plasma like media are placed into the waveguide  $7.2 \times 3.4$  mm as it shown in Fig. 42.

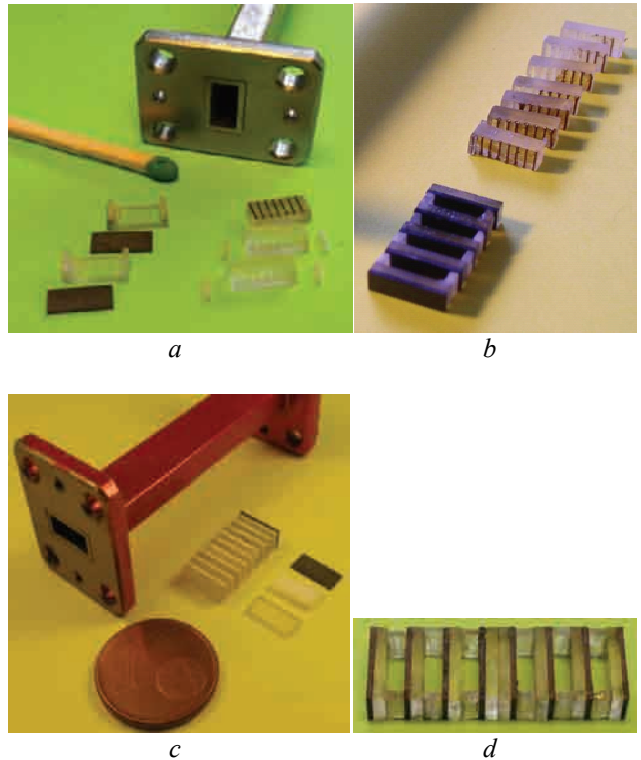


Fig. 42. The MPC crystals for study Tamm states in waveguide regime: MPC bounded with plasma-like medium (the wire-medium)  $\epsilon < 0$  (a,b); PC bounded with ferrite  $\mu < 0$  (c); the mirror-reflected MPC made from ferrite plates  $7.2 \times 3.4$  mm (d).

#### Plasma-like media for PC bounding

Plasma-like media are formed by the set of wires or disks having various geometrical sizes. The elements are deposited onto quartz/teflon/polystyrene substrates.

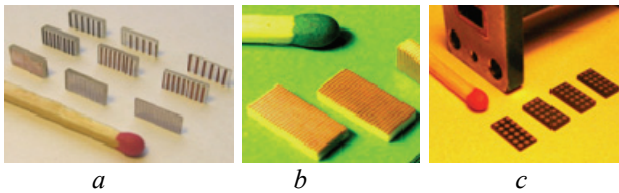


Fig. 43. The elements should be inserted into waveguides: wire-media (the anisotropy plasma-like media) with various density (a,b); disk-media (the isotropy plasma-like media) (c). The plasma frequency of about  $(2-8) \cdot 10^2$  GHz.

*Left handed media for waveguide study*

The structures (Fig. 44) are designed to be placed in a waveguide, so that wave vector was directed normally to the plates plane (case a) and normally to the plate formed by sticks (case b).

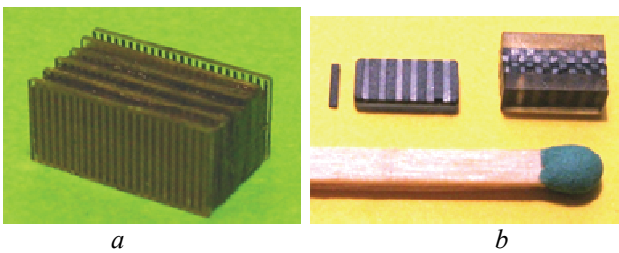


Fig. 44. Samples of magnetically controlled left handed media: Wire-media/ferrite made from plates (a); InSb/ferrite structures made from thin sticks of each element (b). Size of elements satisfied to  $d \ll \lambda$ .

*Prism shaped left handed media*

The prism shaped LHM were placed into T-bridge, Fig. 45,d. Static magnetic field is applied normally to the lateral facet of the prism.

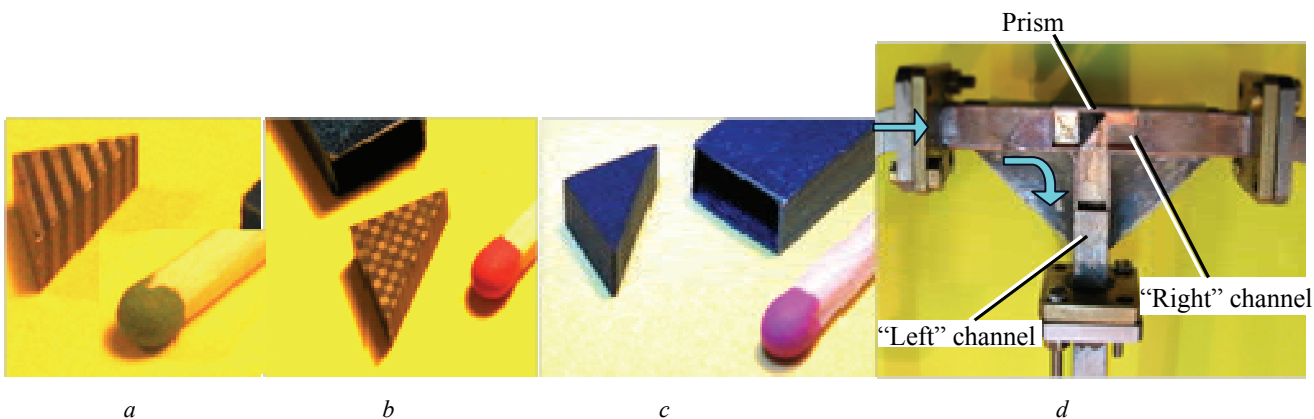


Fig. 45. Left handed media prisms: ferrite/InSb plates and sticks (a,b); the sintered manganite-perovskite powder (c); experimental setup (T-bridge) to detect the negative refraction coefficient with LHM prism inside (d).

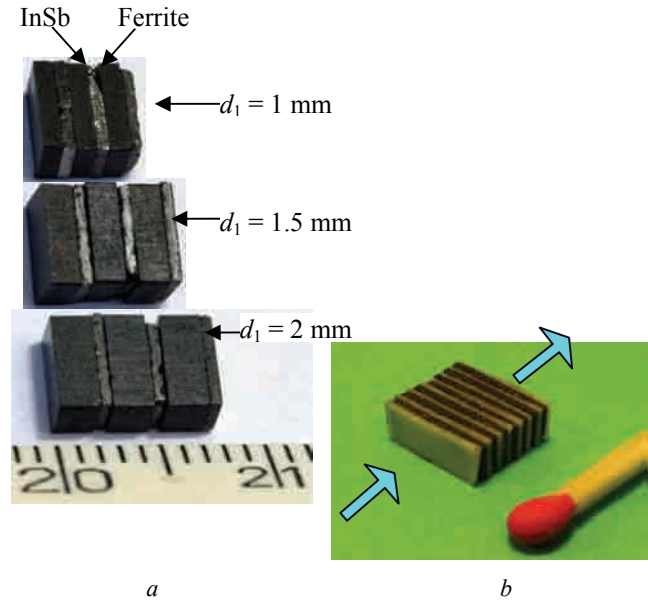


Fig. 46. The structure formed by bilayers: InSb semiconductor/ferrite with various ferrite layer thickness  $d_1$  (a); the fine stratified structure of manganite-perovskite (b).

*The fine-stratified composites*

Typical fine-stratified structures, used for investigation of processes taking place while unit element size becomes smaller than the wavelength are given in Fig. 46.

**Acknowledgement**

Authors thank all numerous co-authors who have brought their definite contribution in fulfillment of investigations entered the review.

Partial financial support for these works was provided by STCU Projects # 3727, #4912, #5210.

1. K. Inoue and K. Ohtaka (eds.), *Photonic Crystals, Physics, Fabrication, Application*, Springer (2004), p. 317.
2. M. Inoue, R. Fujikava, A. Baryshev, A. Khanikaev, P.B. Lim, H. Uchida, O. Aktsiperov, A. Fedyanin, T. Murzina, and A. Granovsky, *J. Phys.* **D39**, R151 (2006).
3. C.M. Krowne and Y. Zang (eds.), *Physics of Negative Refraction and Negative Index Materials*, Springer (2007), p. 378.
4. A.P. Vinogradov, A.V. Dorofeenko, A.M. Merzlikin, and A.A. Lisyansky, *Phys. Usp.* **53**, 243 (2010).
5. A.P. Vinogradov, A.V. Dorofeenko, S.G. Erokhin, M. Inoue, A.A. Lisyansky, and A.B. Granovsky, *Phys. Rev.* **B74**, 045128 (2006).
6. F.G. Bass and A.A. Bulgakov, *Kinetics and Electrodynamics Phenomena in Classical and Quantum Semiconductor Superlattices*, Nova Science, New York (1997).
7. S.V. Chernovtsev, D.P. Belozorov, and S.I. Tarapov, *J. Phys.* **D40**, 295 (2007).
8. A.G. Gurevich, *Magnetic Resonance in Ferrites and Antiferromagnets*, Nauka, Moscow (1973) (in Russian).
9. A.G. Gurevich and G.A. Melkov, *Magnetization Oscillations and Waves*, CRC Press, New York (1996).
10. V.P. Abramov, V.A. Dmitriev, and S.A. Sheluhin, *Nonreciprocal Devices and the Ferrite Resonators*, Radio i Svyaz', Moscow (1989) (in Russian).
11. E.J. Schlomann, *Appl. Phys.* **41**, 204 (1970).
12. J. Green and F. Sandy, *IEEE Trans.* **22**, 641 (1974).
13. O.V. Kostilyova, A.A. Bulgakov, A.A. Girich, A.A. Kharchenko, and S.I. Tarapov, *Proc. XLI European Microwave Conference: EuMC-2011*, Manchester, UK (2011), p. 850.
14. S. Tarapov, D. Belozorov, M. Khodzitsky, and S. Nedukh, in: *Proc. Intern. Workshop Magnetic Phenomena in Micro- and Nano-Structures: MPMNS'10*, Donetsk, Ukraine (2010), p. 20.
15. M. Born and E. Volf, *Principles of Optics*, Pergamon Press, Oxford (1968).
16. S.V. Chernovtsev, *Radiotechnics: Vseukr. Mejved. Nauchn.-Tech. sb.* **150**, 137 (2007) (in Russian).
17. A.G. Gurevich, *Ferrite at Microwaves*, Fizmatgiz, Moscow (1960) (in Russian).
18. D.P. Belozorov, M.K. Khodzitsky, and S.I. Tarapov, *J. Phys.* **D42**, 055003 (2009).
19. M.K. Khodzitsky, T.V. Kalmykova, S.I. Tarapov, D.P. Belozorov, A.M. Pogorily, A.I. Tovstolytkin, A.G. Belous, and S.A. Solopan, *Proc. III Intern. Congr. on Advanced Electromagnetic Materials in Microwaves and Optics: Metamaterials-2009*, London, UK (2009), p. 647.
20. S.I. Tarapov, M.K. Khodzitsky, S.V. Chernovtsev, D.P. Belozorov, A.M. Merzlikin, A.P. Vinogradov, A.B. Granovsky, and M. Inoue, *Solid State Phenomena* **152-153**, 394 (2009).
21. S. Tarapov, M. Khodzitsky, S.V. Chernovtsev, D. Belozorov, A. Merzlikin, A.V. Dorofeenko, A.P. Vinogradov, M. Inoue, and A.B. Granovsky, *Phys. Solid State* **52**, 1427 (2010).
22. M.K. Khodzitsky, O.V. Kostilyova, O.V. Shramkova, A.A. Bulgakov, A.A. Girich, and S.I. Tarapov, *Proc. III Intern. Congr. on Advanced Electromagnetic Materials in Microwaves and Optics: Metamaterials-2009*, London, UK (2009), p. 230.
23. A.A. Girich, M.K. Khodzitsky, O.V. Shramkova, and S.I. Tarapov, *Proc. XL European Microwave Conference*, France (2010), p. 1421.
24. A.A. Bulgakov, A.A. Girich, M.K. Khodzitsky, O.V. Shramkova, and S.I. Tarapov, *J. Opt. Soc. Am.* **B26**, B156 (2009).
25. V.M. Agranovich and Y.N. Gartstein, *Phys. Usp.* **49**, 1029 (2006).
26. A. Boardman, *J. Opt.* **13**, 020401 (2011).
27. V.G. Veselago, *Sov. Phys. Usp.* **10**, 509 (1968).
28. A. Pimenov, A. Loidl, K. Gerke, V. Moshnyaga, and K. Samwer, *Phys. Rev. Lett.* **98**, 197401 (2007).
29. A.G. Belous, O.I. V'yunov, E.V. Pashkova, O.Z. Yanchevskii, A.I. Tovstolytkin, and A.N. Pogorily, *Inorg. Mater.* **39**, 212 (2003).
30. M.K. Khodzitsky, T.V. Kalmykova, S.I. Tarapov, D.P. Belozorov, A.M. Pogorily, A.I. Tovstolytkin, A.G. Belous, and S.A. Solopan, *Appl. Phys. Lett.* **95**, 082903 (2009).
31. D. Belozorov, M. Khodzitsky, P. Belov, and S. Tarapov, *Proc. Intern. Kharkov Symposium on Physics and Engineering of Microwaves, Millimeter and Submillimeter Waves: MSMW'2010*, Kharkov, Ukraine (2010), W-12.
32. M.K. Khodzitsky, A.A. Kharchenko, A.V. Strashkevskiy, and S.I. Tarapov, *Telecommun. Radio Engineering* **68**, 561 (2009).
33. R.H. Tarkhanyan and D.G. Niarchos, *Opt. Express* **14**, 5433 (2006).
34. R. Wu, T. Zhao, and J. Xi, *J. Phys.: Cond. Matter* **19**, 026211 (2007).
35. O.V. Shramkova, *Prog. Electromagn. Res.* **M7**, 71 (2009).
36. Ya.B. Fainberg and N.A. Khizhnyak, *J. Theor. Phys.* **48**, 711 (1955).
37. A.A. Girich, M.K. Khodzitsky, and S. Tarapov, *Proc. III Intern. Congr. on Advanced Electromagn. Mater in Microwaves and Optics: Metamaterials-2009*, London, UK (2009), p. 590.
38. Rui-Xin Wu, Tianen Zhao, and John Q Xiao, *J. Phys.: Cond. Matter* **19**, 026211 (2007).
39. E.Yu. Al'tshuler and I.S. Nefedov, *J. Commun. Tech. Electronics* **53**, 57 (2008).
40. A.A. Girich and S.I. Tarapov, *Proc. V Intern. Congress on Advanced Electromagnetic Materials in Microwaves and Optics: Metamaterials'2011*, Barcelona, Spain (2011), p. 447.
41. H. Chen, L. Ran, J. Huangfu, X. Zhang, K. Chen, T.M. Grzegorzczak, and J.A. Kong, *J. Appl. Phys.* **94**, 3712 (2003).
42. R.W. Ziolkowski and E. Heyman, *Phys. Rev.* **E64**, 056625 (2001).
43. A.A. Girich and S.I. Tarapov, *Proc. Intern. Workshop on Terahertz and Mid-Infrared Radiation: Basic Research: TERA-MIR -2009*, Turkey (2009), p. 65.
44. J.B. Pendry, A.J. Holden, D.J. Robbins, and W.J. Stewart, *J. Phys.: Cond. Matter* **10**, 4785 (1998).
45. S.V. Vonsowsky, *Magnetism*, Wiley, New York (1974).
46. A.I. Tovstolytkin, A.M. Pogorily, D.I. Podyalovskii, V.M. Kalita, A.F. Lozenko, P.O. Trotsenko, S.M. Ryabchenko, A.G. Belous, O.I. V'yunov, and O.Z. Yanchevskii, *J. Appl. Phys.* **102**, 063902 (2007).

47. V.G. Bar'yakhtar, A.N. Pogorily, N.A. Belous, and A.I. Tovstolytkin, *J. Magn. Magn. Mater.* **207**, 118 (1999).
48. A.-M. Haghiri-Gosnet and J.-P. Renard, *J. Phys.* **D36**, 127 (2003).
49. T. Goto, A.V. Dorofeenko, A.M. Merzlikin, A.V. Baryshev, A.P. Vinogradov, M. Inoue, A.A. Lisyansky, and A.B. Granovsky, *Phys. Rev. Lett.* **101**, 113902 (2008).
50. A. Namdar, I.V. Shadrivov, and Y.S. Kivshar, *J. Appl. Phys. Lett.* **89**, 114104 (2006).
51. M.K. Khodzitsky, S.I. Tarapov D.P. Belozorov, A.M. Pogorily, A.I. Tovstolytkin, A.G. Belous, and S.A. Solopan, *Appl. Phys. Lett.* **97**, 131912 (2010).
52. C. Kittel, *Introduction to Solid State Physics*, Wiley, New-York (1996).
53. P.V. Parimi, W.T. Lu, P. Vodo, J. Sokoloff, J.S. Derov, and S. Sindhar, *Phys. Rev. Lett.* **92**, 127401 (2004).
54. D.P. Belozorov, T.V. Kalmykova, S.I. Tarapov, A.M. Pogorily, A.I. Tovstolytkin, A.G. Belous, and S.A. Solopan, *Appl. Phys. Lett.* **100**, 171104 (2012).